How to cite: *Angew. Chem. Int. Ed.* **2024**, *63*, e202319978
doi.org/10.1002/anie.202319978

Gas Separation | Hot Paper

Scalable Synthesis of Robust MOF for Challenging Ethylene Purification and Propylene Recovery with Record Productivity

Gang-Ding Wang[+], Yong-Zhi Li[+], Rajamani Krishna, Wen-Yan Zhang, Lei Hou, Yao-Yu Wang, and Zhonghua Zhu*

Abstract: Ethylene (C_2H_4) purification and propylene (C_3H_6) recovery are highly relevant in polymer synthesis, yet developing physisorbents for these industrial separation faces the challenges of merging easy scalability, economic feasibility, high moisture stability with great separation efficiency. Herein, we reported a robust and scalable MOF (MAC-4) for simultaneous recovery of C_3H_6 and C_2H_4. Through creating nonpolar pores decorated by accessible N/O sites, MAC-4 displays top-tier uptakes and selectivities for C_2H_6 and C_3H_6 over C_2H_4 at ambient conditions. Molecular modelling combined with infrared spectroscopy revealed that C_2H_6 and C_3H_6 molecules were trapped in the framework with stronger contacts relative to C_2H_4. Breakthrough experiments demonstrated exceptional separation performance for binary C_2H_6/C_2H_4 and C_3H_6/C_2H_4 as well as ternary $C_3H_6/C_2H_6/C_2H_4$ mixtures, simultaneously affording record productivities of 27.4 and 36.2 L kg^{-1} for high-purity C_2H_4 ($\geq$99.9 %) and C_3H_6 ($\geq$99.5 %). MAC-4 was facilely prepared at deckgram-scale under reflux condition within 3 hours, making it as a smart MOF to address challenging gas separations.

Introduction

Global demand for propylene (C_3H_6) and ethylene (C_2H_4) which are important chemical feedstocks in downstream manufacture industry is increasing,[1,2] with a total global production of beyond 300 million tons in 2023.[3,4] C_3H_6 and C_2H_4 are traditionally produced from the crude oil cracking or dehydrogenation process. Considerable attention has been recently paid to producing C_3H_6 and C_2H_4 from natural gas, coal, biomass, and methanol-to-olefins (MTO) reaction.[5] In these processes, C_2H_4 products inevitably comprise small of ethane (C_2H_6) impurities at 6–10 %, while the products of MTO reaction mainly contain C_3H_6 of 20.9 wt % and C_2H_4 of 51.1 wt %.[6,7] Therefore, the follow-up separation by cryogenic distillation cycling operated under high pressure and low temperature conditions is essential to derive polymer-grade olefins since their highly close physicochemical properties.[8–10] Replacing distillation technology by adsorption separation using porous adsorbents would bring tremendous global benefits due to high efficiency, energy saving, and environmental friendliness.[11–13]

Metal–organic frameworks (MOFs) as an emerging type of customizable adsorbents with abundant functionality and structural modularity offer a promising platform for addressing the task-specific requirements of various applications,[14–18] especially in gas separation and purification.[19–24] For C_2H_6/C_2H_4 separation, the utilization of C_2H_6-selective MOFs is more desirable owing to pure C_2H_4 products can be directly obtained through one-step separation process, avoiding additional desorption step that is indispensably for C_2H_4-selective MOFs and greatly reducing energy consumption.[25–28] However, C_2H_6-selective MOFs were not well developed, in particularly they usually suffer from "trade-off" effect with either low selectivity because of the difficulty in discriminating C_2H_4 and C_2H_6 or low adsorption capacity owing to small available voids.[29,30] This trouble makes it be a constant challenge in designing C_2H_6-selective MOFs.

The latest research demonstrated that the creation of open metal sites (OMSs) in MOFs is effective for C_3H_6/C_2H_4 separation, wherein the OMSs bind the C=C π units in C_3H_6 and C_2H_4 by M···π interactions with different strengths.[7,31] However, this strategy is not judicious for designing C_2H_6-selective MOFs since C_2H_4 are more easily adsorbed by OMSs. As high contents of C_2H_4 and C_3H_6 in MTO products, the collection of high-purity C_2H_4 and C_3H_6 through separating C_3H_6/C_2H_4 mixtures is important for the

[*] Dr. G.-D. Wang,[+] Dr. Y.-Z. Li,[+] Prof. W.-Y. Zhang, Prof. L. Hou, Prof. Y.-Y. Wang
Key Laboratory of Synthetic and Natural Functional Molecule of the Ministry of Education
College of Chemistry & Materials Science, Northwest University
Xi'an, 710069, P. R. China.
E-mail: lhou2009@nwu.edu.cn
Prof. R. Krishna
Van't Hoff Institute for Molecular Sciences University of Amsterdam
Science Park 904, 1098 XH Amsterdam, The Netherlands
Dr. Y.-Z. Li[+]
School of Materials and Physics, China University of Mining and Technology
Xuzhou 221116, P. R. China.
Prof. Z. Zhu
School of Chemical Engineering, The University of Queensland
Brisbane 4072, Australia
[+] These authors contributed equally to this work.

downstream application of olefins. However, at present the simultaneous recovery of C_3H_6 and C_2H_4 by MOFs was only reported in one example.[32] So it is of great industrial and academic interest to develop the MOFs for separating both C_2H_6/C_2H_4 and C_3H_6/C_2H_4 mixtures to afford pure C_2H_4 and C_3H_6, respectively. Besides, the real challenge remaining for C_2H_4 purification technology through MOFs could lie in the scale-up synthesis and affordable cost of the materials upon maintaining the separation performance. Currently, most of the reported C_3H_6- or C_2H_6-selective MOFs suffer from high production cost, poor stability or synthesis scalability, severely hindering their practical utilization. To data, the efficient C_3H_6- and C_2H_6-selective MOFs that satisfied all the above requirements have not been reported. Thus, it is extremely essential to develop MOFs that merge the factor regarding to excellent separation performance, while remains a daunting challenge.

A handful of C_2H_6-selective MOFs containing nonpolar pore surfaces (e.g., aliphatic or aromatic moieties) have been recently evidenced to be certainly beneficial for preferentially adsorbing C_2H_6 over C_2H_4 based on the slightly higher polarizability of C_2H_6 (44.7×10^{25} cm^{-3}) over C_2H_4 (42.52×10^{25} cm^{-3}).[25,33] In addition, there were also some MOFs that mainly relied on well-designed available interacting sites (e.g. N/O atoms), leading to more hydrogen bonds with C_2H_6 and C_3H_6 than C_2H_4.[34,35] With the above considerations in mind, we supposed that design nonpolar pore environments with N/O active sites in MOFs could display the potential for both C_2H_6/C_2H_4 and C_3H_6/C_2H_4 separation. Herein, we developed a highly stable MOF, MAC-4 [$Zn_5(dmtrz)_3(ipa)_3(OH)$], fabricated by Zhou et al.[36] This material is composed of inexpensive and easily available ligands of isophthalic acid (H_2ipa) and 3,5-dimethyl-1,2,4-triazole (Hdmtrz) ligands. In particular, it contains nonpolar pores with rich O/N sites and inorganic secondary building units (SBUs) without undesired OMSs, these two structure features would be very favourable for the target function of C_2H_6- and C_3H_6 selectivity over C_2H_4 in MOFs. MAC-4 displayed not only high uptakes and selectivities for C_2H_6 and C_3H_6 over C_2H_4 but also efficient one-step purification of C_2H_4 from C_2H_6/C_2H_4 and C_3H_6/C_2H_4 mixtures with high C_2H_4 productivity of 21.6 L kg^{-1} and 349.3 L kg^{-1}, respectively. MAC-4 also provided a record high C_3H_6 ($\geq$99.5 %) recovery capacity of 70.1 L kg^{-1} in single C_3H_6/C_2H_4 separation process, as well as one-step acquisition of C_2H_4 ($\geq$99.9 %) and C_3H_6 ($\geq$99.5 %) from $C_3H_6/C_2H_6/C_2H_4$ mixtures. GCMC calculations unveiled that multiple N/O active sites in nonpolar pores provided stronger interactions with both C_3H_6 and C_2H_6 over C_2H_4.

Results and Discussion

MAC-4 with an orthorhombic *Pnma* space group was built on two types of cluster-based SBUs: paddle-wheel [$Zn_2(COO)_4$] and triangle [$Zn_3(OH)(dmtrz)_3$]. The same SBUs are connected by ipa^{2-} linkers or Zn–N coordination bonds to produce one-dimensional chains along the *b* and *a* axes, respectively (Figure 1a and S1). The linkage between two types of SBUs through coordination interactions generates a 3D porous network. Remarkably, the framework with the void of ~45.5 % contains 1D zig-zag open channels (size ~5.9–8.0 Å) that were decorated by the methyl groups of dmtrz, phenyl rings of ipa^{2-} ligands as well as rich N and O sites (Figure 1b and 1c).

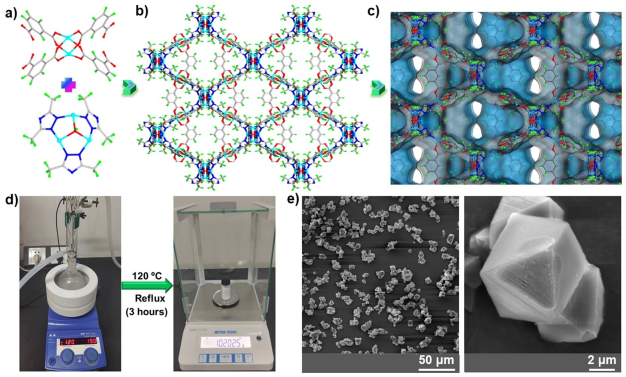

Figure 1. a) [$Zn_2(COO)_4$] and [$Zn_3(OH)(dmtrz)_3$] SBUs, b) and c) 3D structure of MAC-4 (H, green; Zn, turquoise; C, gray; O, red; N, blue); d) photographs of the deckgram-scale synthesis of MAC-4; e) SEM images of MAC-4 microcrystalline with octahedral bulk.

In the pursuit of convenient synthesis methods, it was important to find that MAC-4 could be rapidly and easily synthesized through refluxing the reactants in DMF within 3 hours with a high yield (78 %). The phase purity and crystallinity of the MAC-4 microcrystalline were verified by scanning electron microscope (SEM) and powder X-ray diffraction (PXRD) tests (Figure 1d, 1e and S2). Thermogravimetric analysis (TGA) displayed a continuous weight loss; however, the CH_2Cl_2-exchanged samples showed a wide thermostable plateau up to 350 °C following an initial weight loss before 140 °C (Figure S3).

Nitrogen (N_2) adsorption isotherms at 77 K showed type-I curves for the scaled-up and single-crystal MAC-4 samples with the saturated loadings of 338 and 343 cm^3 g^{-1}, respectively, indicating the close Brunauer–Emmett–Teller (BET) surface areas of 1180 and 1218 m^2 g^{-1} (Figure S4). The pore size distribution of 6.4–10.8 Å agrees with the calculated results from crystal structure. The accessible porous wall of MAC-4 is mainly modified by phenyl rings and methyl groups in ligands, giving rise to a hydrophobic environment, as confirmed by the water vapour adsorption showing a type-V isotherm at 298 K (Figure S5). The structure of MAC-4 after both activation and water adsorption was intact, as demonstrated by PXRD (Figure S2).

The suitable pore size and nonpolar pore environment of MAC-4 inspired us to examine its C_2H_4 purification performance. First, the sorption isotherms of different shape of MAC-4 samples prepared from solvothermal (crystals) and reflux (microcrystalline) reactions were measured at 273 and 298 K (Figure S6–S8). Both samples displayed very close sorption isotherms for C_2H_6, C_2H_4, and C_3H_6, demonstrated no difference in adsorption performance between the samples. MAC-4 showed typical type-I sorption iso-

therms for C_2H_6, C_2H_4, and C_3H_6 with the uptakes of 107/124, 83/108, and 127/140 $cm^3 g^{-1}$ at 100 kPa and 298/273 K, respectively (Figure 2a and S9). The C_2H_6 uptake in MAC-4 is remarkably higher than most top-performing C_2H_6-selective materials, such as MUF-15,[37] Azole-Th-1,[38] NKCOF-21,[39] TJT-100,[30] $Fe_2(O_2)$dobdc,[40] MAF-49[41] and so on, and is slightly lower than benchmark MOFs CPM-233[42] and ZJU-120a[43] (Figure S10). MAC-4 also shows exceptional loadings of 56, 42, and 108 $cm^3 g^{-1}$ for C_2H_6, C_2H_4, and C_3H_6 at a high temperature of 353 K (Figure 2b). Meanwhile, the adsorption curves of MAC-4 exhibit higher uptakes and steeper slopes for C_3H_6 and C_2H_6 than C_2H_4, indicating selective adsorption of C_3H_6 and C_2H_6 over C_2H_4. These findings are in accord with the calculated values of adsorption enthalpy (Q_{st}) at zero coverage with the order of C_3H_6 (25.3 kJ mol^{-1}) > C_2H_6 (22.7 kJ mol^{-1}) > C_2H_4 (17.1 kJ mol^{-1}) (Figure 2c). It was noted that the Q_{st} data showed inflection points for three gases, in particular for C_3H_6 and C_2H_6, from zero-coverage to 1.5, 1.0, and 1.0 mmol g^{-1} loadings for C_3H_6, C_2H_6, and C_2H_4 gases, respectively, which corresponded to the amounts of gas molecules in one pore were about 1.7, 1, and 1 molecules. The inflection points for Q_{st} data could be because of the reorientation of gas molecules in pores under increased pressure. Meanwhile, due to relatively high loadings, the interactions between the C_3H_6 molecules in pores could also be responsible for the obviously increased Q_{st} of C_3H_6.[37] Notably, the Q_{st} values of three gases are below 32 kJ mol^{-1} owing to the nonpolar pores of MAC-4, implying a facile regeneration treatment with low energy consumption. In fact, the fully reproducible C_3H_6, C_2H_6, and C_2H_4 adsorption curves can be recycled with the simple activation treatment (353 K for 10 minutes) prior to each cycle (Figure S11–13).

Given that the real-industrial application environment, the material must possess long-term and high humidity stability. The stability of MAC-4 toward air environments and humidity was evaluated and monitored by gas adsorptions and PXRD measurements. As divulged in Figure 2d (left), after exposing to 65 % humidity and air environment for 60 days, MAC-4 remains intact without crystallinity loss and phase transformation, as verified by PXRD. Moreover, the adsorption isotherms for C_2H_6 at 298 K for above samples are very close to that of the initial samples, confirming and guaranteeing the great stability of MAC-4 for practical utilization (Figure 2d right).

As for higher uptakes and larger adsorption enthalpies toward C_3H_6 and C_2H_6 than C_2H_4, the separation selectivities of MAC-4 for C_2H_6/C_2H_4 and C_3H_6/C_2H_4 mixtures were evaluated by employing ideal adsorbed solution theory (Figure S14–S16). For C_2H_6/C_2H_4 mixtures, MAC-4 displays high initial selectivities of 2.0/2.3/3.8, 2.0/2.4/4.1, and 2.0/2.4/4.2 for 1/1, 1/9, and 1/15 mixtures at 353/298/273 K, respectively, and which are still high of 1.7/1.9/2.2 at 100 kPa (Figure 3a, S17, and S19). These selectivities are higher than or comparable to many well-developed C_2H_6-selective adsorbents, e.g. SNNU-40,[44] CPOC-301,[45] NKCOF-22,[39] and TJT-100.[30] For C_3H_6/C_2H_4 mixtures, the selectivity values were calculated to be 8.6/9.5/16.2, 8.4/10.6/19.2, and 8.1/10.9/20.6 for 1/1, 2/5, and 1/9 C_3H_6/C_2H_4 mixtures at 353/298/273 K, respectively (Figure 3b, S18, and S19), which are only lower than $Zn_2(oba)_2(dmipym)$,[34] but significantly larger than most of materials, such as Mn-dpzip,[31] NEM-7-Cu,[46] and Zn-BPZ-SA[35] (Figure S20). At the same time, the separation potential (ΔQ) that was reported by Krishna and integrated the advantages of selectivity and capacity was utilized to evaluate the separation performance, which reflects the maximum C_2H_4 productivity.[47,48] For equimolar C_2H_6/C_2H_4 mixtures, ΔQ were calculated to be 0.5, 1.3, and 1.9 mmol g^{-1} at 353, 298, and 273 K, respectively (Figure S21), outdoing the most advanced C_2H_6-selective adsorbents, such as MUF-15,[37] NKCOF-23,[39] CPOC-301,[45] and Tb-MOF-76(NH_2),[49] under the same conditions (Figure 3c). The corresponding ΔQ values for equimolar C_3H_6/C_2H_4 mixtures are 3.2, 4.4, and 5.3 mmol g^{-1} at 353, 298, and 273 K, respectively (Figure S22), superior to some well-

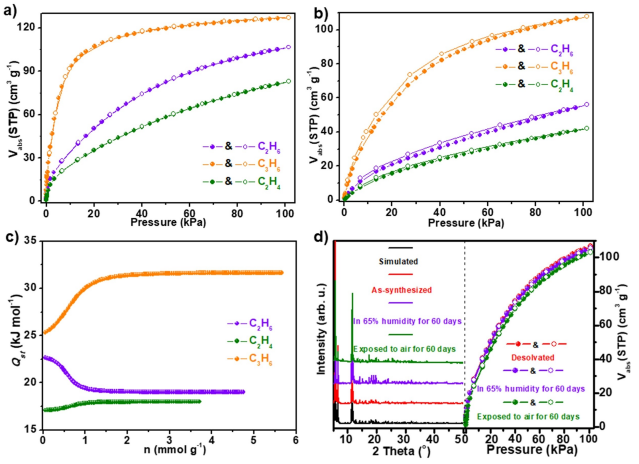

Figure 2. a) Sorption isotherms of MAC-4 at 298 K; b) sorption isotherms of MAC-4 at 353 K; c) Q_{st} curves; d) PXRD patterns (left) and C_2H_6 adsorption isotherms (right) of MAC-4 samples.

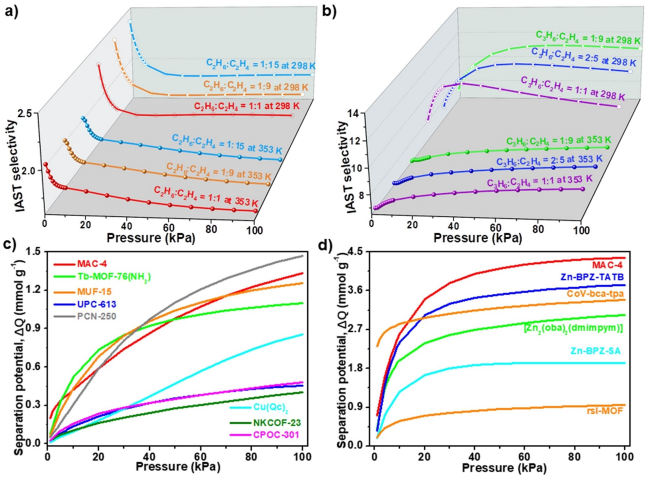

Figure 3. a) and b) IAST selectivities of MAC-4 for C_2H_6/C_2H_4 and C_3H_6/C_2H_4 mixtures; comparisons of separation potential for C_2H_6/C_2H_4 (c) and C_3H_6/C_2H_4 (d) mixtures in MAC-4 and other adsorbents at 298 K.

developed MOFs, e.g. $[Zn_2(oba)_2(dmimpym)]$,[34] Zn-BPZ-SA,[35] CoV-bca-tca,[50] and Zn-BPZ-TATB[32] (Figure 3d).

To gain precise insight into the preferential adsorption sites of C_3H_6, C_2H_4, and C_2H_6 in MAC-4, molecular modelling was performed based on Grand Canonical Monte Carlo (GCMC) simulations. All three gas molecules were preferentially located at the cavities formed around two $[Zn_2(COO)_4]$ SBUs and two triazolate-trinuclear $[Zn_3(OH)(dmtrz)_3]$ SBUs. One C_2H_4 interacts with three carboxylate O atoms and two triazolate N atoms through quintuple C–H···O/N hydrogen bonds (H···O/N = 2.88–3.19 Å) (Figure 4a). In comparison, the interactions between the framework and C_3H_6/C_2H_6 molecules are more and stronger, in which C_2H_6 is bound to four N atoms from $[Zn_3(OH)(dmtrz)_3]$ SBUs and three O atoms through seven C–H···O/N hydrogen bonds (H···O = 2.85–3.19 Å) (Figure 4b). For C_3H_6, it not only is involved in nine C–H···O/N hydrogen bonds (H···O = 2.79–3.26 Å), but also forms one C–H···π interaction via the alkenyl π clouds of C_3H_6 (Figure 4c). Therefore, the MOF possesses a greater affinity for C_2H_6 and C_3H_6 relative to C_2H_4. Meanwhile, the calculated binding energies also showed larger values for C_3H_6 (37.3 kJ mol^{-1}) and C_2H_6 (35.7 kJ mol^{-1}) compared to C_2H_4 (31.5 kJ mol^{-1}).

The interactions of C_2H_4, C_3H_6, and C_2H_6 with MAC-4 were deliberated at 100 kPa and 298 K by further simulations. As divulged in Figure S23–S26, two C_2H_4, three C_2H_6, and four C_3H_6 molecules mainly interacted with the pore walls. Two C_2H_4 via the -CH units form multiple C–H···O/N contacts with triazolate N atoms and carboxylate O atoms (Figure S23). Three C_2H_6 molecules are located in different coordination fragments interacting with N/O atoms through C–H···O/N hydrogen bonds (H···O/N = 2.65–3.29 Å) (Figure S24). C_3H_6 molecules are involved in more contacts not only with the accessible N/O atoms but also with the π centers and methyl groups from linkers. Specifically, C_3H_6-I and C_3H_6-II exist in similar locations around two $[Zn_2(COO)_4]$ SBUs through C–H···O/π contacts (H···O = 2.69–3.17 Å, H···π = 2.86–3.32 Å) with carboxylate O atoms and phenyl π centers as well as C–H···π interactions between two C_3H_6 molecules (Figure S25). C_3H_6-III and C_3H_6-IV are resided in the region of $[Zn_3(OH)(dmtrz)_3]$ fragments through forming multiple C–H···C/O/N hydrogen bonds and C–H···π interactions with the ligands (Figure S26). Meanwhile, these multiple contacts for C_3H_6 and C_2H_6 molecules can also be confirmed by the higher values of interaction energy (E) distributions for C_3H_6 ($\bar{E}$ = 56.9 kJ mol^{-1}) and C_2H_6 ($\bar{E}$ = 41.8 kJ mol^{-1}) compared to C_2H_4 ($\bar{E}$ = 34.7 kJ mol^{-1}) (Figure S27). The simulation results are in accordance with the experimental findings and well explain the high selectivities for both C_3H_6 and C_2H_6 over C_2H_4.

Breakthrough experiments were performed at 273, 298, and 353 K for C_2H_6/C_2H_4 (v/v, 5/5, 1/9, and 1/15) mixtures under Ar as the carrier gas (vol %, 90 %, 90 % and 84 %, a total flow of 7 mL min^{-1}), in which the mixtures were passed through the packed column. As shown in Figure 5a–5c, three mixtures can be completely separated by MAC-4, in which C_2H_4 was first outflowed from the column to directly get pure C_2H_4 (≥ 99.9 %), while C_2H_6 was adsorbed in the bed for a certain period of times. During this process, 1 kg MAC-4 can retrieve high-purity C_2H_4 (≥ 99.9 %) about 5.4, 14.9, and 21.6 L from 5/5, 1/9, and 1/15 C_2H_6/C_2H_4 mixtures at 298 K, respectively. The breakthrough experiments for the higher concentrations of C_2H_6/C_2H_4 mixtures (10/10, 20/20, 30/30, v/v) were also tested at 273 and 298 K (Figure S28–S30), and it also displayed the complete separation of the mixtures. Moreover, the cycling experiments showed no loss of separation ability in MAC-4, illustrating outstanding reusability (Figure S31).

The difficult scalability and high cost of MOF adsorbents has long been a troubled issue for their application. In general, the cost of MOFs primarily depends on ligands. Although some MOFs display benchmark performance for C_2H_6/C_2H_4 separation, they suffer from long-time (48–72 h)

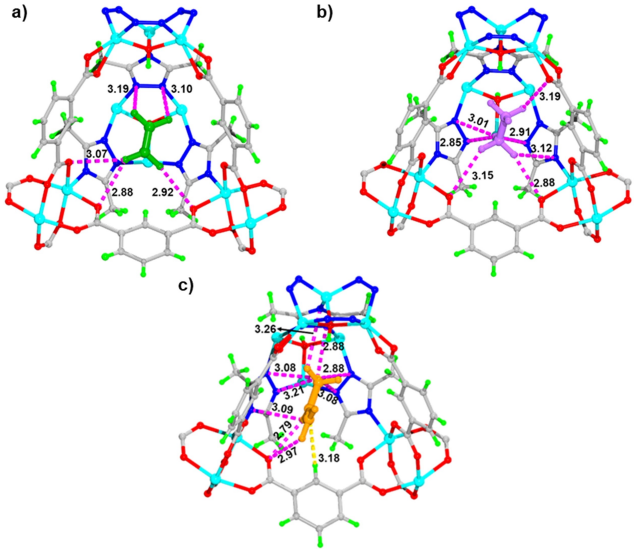

Figure 4. Preferential adsorption sites for a) C_2H_4, b) C_2H_6, and c) C_3H_6 (H, green; Zn, turquiose; C, gray; O, red; N, blue).

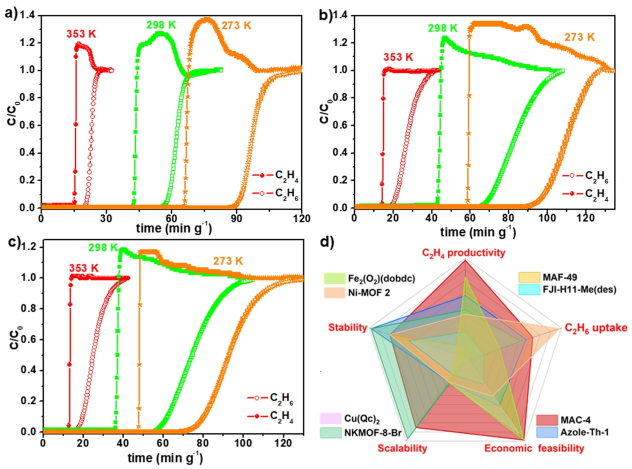

Figure 5. a–c) Breakthrough curves for C_2H_6/C_2H_4 mixtures at 273, 298, and 353 K: a) 1/1, b) 1/9, c) 1/15; d) comprehensive comparisons for MAC-4 and other porous materials.

heating synthesis conditions and the use of expensive ligands, such as 2-bromoimidazole-4,5-dicarbonitrile of NKMOF-8-Br (142 $ g^{-1}), 2,3,5,6-tetramethylterephthalic acid of Ni(TMBDC)(DABCO)$_{0.5}$ (309 $ g^{-1}), 4-(1H-tetrazol-5-yl) benzoic acid of Azole-Th-1 (62 $ g^{-1}), and 4,4′,4″,4‴-(ethene-1,1,2,2-tetrayl) tetrabenzoic acid of NUM-7a (309 $ g^{-1}).[28] In contrast, MAC-4 could be facilely deck-gram-scalably prepared through stirring within 3 hours from commercially available cheap reagents with a cost of about 1 $ g^{-1} (Table S2). Taken together, MAC-4 not only displays promising C_2H_6/C_2H_4 separation performance, but also satisfies several crucial criteria for an industrial adsorbent including high stability, scalability, and economic feasibility, rendering it to be one of benchmark material to address challenges on C_2H_4 purification in industrial application (Figure 5d).

The breakthrough experiments for various ratios of C_3H_6/C_2H_4 (v/v: 20/20, 10/25, and 4/36) mixtures with Ar as carrier gas (vol %: 60 %, 65 %, and 60 %) were also conducted to appraise the separation for MTO products. As presented in Figure 6a, 6b, S32, S33 and S34, highly efficient separation for the mixtures can be achieved by MAC-4, whereby C_2H_4 eluted through the column to directly yield an outflow of pure C_2H_4 (≥ 99.9 %), but C_3H_6 was adsorbed for a long time. About 125.1, 210.6, and 349.3 L of pure C_2H_4 (≥ 99.9 %) could be trapped from 20/20, 10/25, and 4/36 C_3H_6/C_2H_4 mixtures, respectively, for 1 kg MAC-4 at 298 K in one cycle, surpassing all-known C_3H_6-selective adsorbents, such as iso-MOF-4,[7] [Zn_2(oba)$_2$(dmimpym)],[34] Fe_2Mn–L,[51] and Zn-BPZ-SA.[35] As C_3H_6 is another target gas that needs to be purified from MTO products, the desorption experiments were then performed to determine C_3H_6 purity and productivity. Upon reaching equilibrium concentration, the adsorption-saturated MAC-4 was purged by Ar gas-(7 ml min^{-1})at 323 K. As shown in Figure 6a and 6b, the

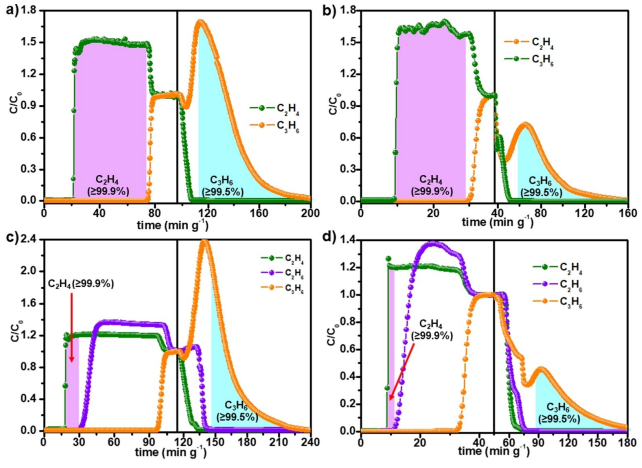

Figure 6. a) Breakthrough curves for C_3H_6/C_2H_4 (v/v, 20/20) mixtures at 298 K; b) breakthrough curves for C_3H_6/C_2H_4 (v/v, 20/20) mixtures at 353 K; c) breakthrough curves for the $C_2H_6/C_3H_6/C_2H_4$ mixture (v/v/v, 2/10/25) mixtures at 298 K; d) breakthrough curves for the $C_2H_6/C_3H_6/C_2H_4$ mixture (v/v/v,2/10/25) mixtures at 353 K, after adsorption-saturated, the desorption curves obtained under Ar (7 mL min^{-1}) sweeping at 323 K.

samples can be easily regenerated, in which the adsorbed C_2H_4 was desorbed more quickly than C_3H_6 owing to weaker binding affinity of MAC-4 for C_2H_4. It was estimated that 36.8 and 70.1 L kg^{-1} of C_3H_6 (≥ 99.5 %) could be produced from C_3H_6/C_2H_4 (v/v, 20/20) mixtures at 353 and 298 K, respectively. To our best knowledge, these productivities of C_2H_4 and C_3H_6 obtained through MAC-4 separation are highest in reported materials.

Although MAC-4 achieved efficient C_2H_4 purification and C_3H_6 recovery from binary C_3H_6/C_2H_4 mixtures, there are tremendous current impediments and challenges in the recovery of high-valuable C_3H_6 from MTO products due to that typically contains few other light hydrocarbons. Thus, the separation experiments for ternary $C_2H_6/C_3H_6/C_2H_4$ (v/v/v, 2/10/25 and 5/5/5) mixtures at 353 and 298 K were tested. For the 2/10/25 $C_2H_6/C_3H_6/C_2H_4$ mixtures at 298 K, it showed that at the column outlet highly pure C_2H_4 (≥ 99.9 %) flowed out firstly, with a 27.4 L kg^{-1} productivity, following by C_2H_6 after 29.5 min g^{-1}, while C_3H_6 was retained in the column as long as 95.8 min g^{-1}. After adsorption saturation, the desorption steps were carried out by purging with Ar gas (7 ml min^{-1}) at 323 K to evaluate the feasibility of C_3H_6 recovery. As depicted in Figure 6c, C_2H_4 and C_2H_6 were rapidly desorbed from MAC-4 within 30 min g^{-1}, then the high-purity C_3H_6 (≥ 99.5 %) with a 36.2 L kg^{-1} productivity was recovered. Therefore, the pure C_3H_6 and C_2H_4 with record-high productivities can be respectively obtained from $C_2H_6/C_3H_6/C_2H_4$ mixtures in one single adsorption/desorption operation. Furthermore, when the ratios of mixtures were adjusted to 5/5/5 or the temperature was rose to 353 K, MAC-4 still exhibited prominent separation ability (Figure 6d, S35, and S36). These results evidently demonstrated that MAC-4 might deliver pure both C_2H_4 and C_3H_6 from imitative MTO products. Furthermore, multiple breakthrough tests demonstrated no decrease of separation performance at least five continuous cycles (Figure S37), confirming good regeneration of MAC-4. Overall, MAC-4 combines the advances of benchmark C_2H_6/C_2H_4 and C_3H_6/C_2H_4 separation performance, ultrahigh moisture stability as well as scale-up synthesis, making it an outstanding adsorbent for C_2H_4 purification and C_3H_6 recovery application.

Next, transient breakthrough simulations were carried out for the exact same set of operating conditions as in the above mentioned experiments, using the methodology described in earlier publications.[52–55] In these simulations, intra-crystalline diffusion influences are ignored. There is good match between the experiments and simulations in every case (Figure S38–S45). Having established the accuracy of the transient breakthrough simulations, transient breakthrough simulations for the C_2H_6/C_2H_4 (50/50, v/v), C_3H_6/C_2H_4 (50/50, v/v), and $C_3H_6/C_2H_6/C_2H_4$ (33.33/33.33/33.33, v/v/v) mixtures without inert gas were performed at 298 and 353 K and 100 kPa to evaluate the practical applications for C_2H_4 purification of MAC-4. The results in Figure 7 clearly demonstrate that MAC-4 is capable of separating three mixtures, whereby C_2H_4 elutes first in all cases and subsequently reached a plateau to produce polymer-grade C_2H_4 before C_2H_6 and C_3H_6 breakthrough

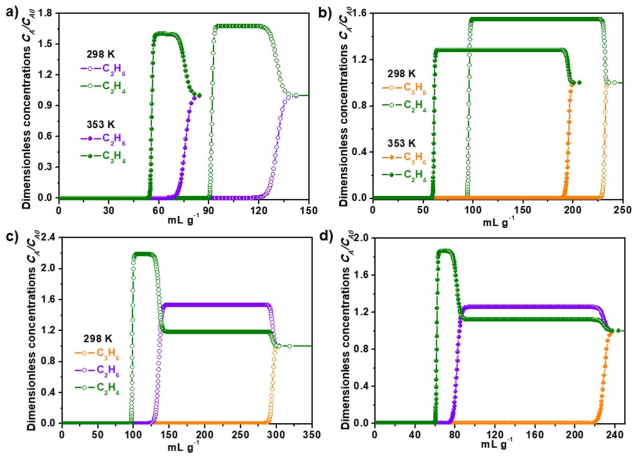

Figure 7. a) Simulated breakthrough curves of MAC-4 for C_2H_6/C_2H_4 (50/50) at 298 and 353 K; b) C_3H_6/C_2H_4 (50/50) at 298 and 353 K; c) $C_3H_6/C_2H_6/C_2H_4$ (33.33/33.33/33.33) at 298 K; d) $C_3H_6/C_2H_6/C_2H_4$ (33.33/33.33/33.33) at 353 K, the *x*-axis is not min g^{-1} but mL g^{-1}.

occurred. Based on the simulated breakthrough curves, MAC-4 can directly produce 8.2, 64.5, and 5.9 L kg^{-1} C_2H_4 (purity >99.9 %) from C_2H_6/C_2H_4, C_3H_6/C_2H_4, and $C_3H_6/C_2H_6/C_2H_4$ at 353 K, respectively. The corresponding C_2H_4 productivity values at 298 K are 23.6, 94.3, and 18.9 L kg^{-1}, respectively. The C_2H_4 productivity for C_2H_6/C_2H_4 (50/50, v/v) are obviously higher than most C_2H_6-selective adsorbents, such as $Fe_2(O_2)$dobdc[40] and JNU-2,[56] Ni-MOF 2,[25] HOF-76a,[57] MAF-49,[41] NKMOF-14-PD,[58] and HOF-NBDA-(DMA)[59] (Figure S46).

In addition, the separation performance of MAC-4 was explored at a crucial low pressure by the simulated density distributions of equimolar binary C_2H_6/C_2H_4 and C_3H_6/C_2H_4 mixtures as well as ternary $C_3H_6/C_2H_6/C_2H_4$ mixtures. As predicted in Figure 8a and 8b, for the inlet of binary C_2H_6/C_2H_4 or C_3H_6/C_2H_4 mixtures under 20 kPa, the density distributions of mixture gases are concentrated at the corners of ipa^{2-} ligands and methyl group near the coordinated units in the framework. Although single-component adsorption site simulation results show that the coordinated units interact with C_2H_4, but for the mixtures the adsorption sites are more occupied by C_3H_6 or C_2H_6 molecules compared to C_2H_4. These findings coincided with the preferentially competitive adsorption for C_3H_6 and C_2H_6 molecules in the framework. Meanwhile, for $C_3H_6/C_2H_6/C_2H_4$ mixtures at 15 kPa, the density distributions of three gas molecules also deferred to the order of $C_3H_6 > C_2H_6 \gg C_2H_4$ (Figure 8c), revealing the preferential adsorption and significant selectivity for C_3H_6 and C_2H_6 over C_2H_4, which further verified the excellent separation performance of MAC-4.

To further probe the gas binding sites, infrared (IR) spectroscopies of MAC-4 with the loading of C_3H_6, C_2H_6, and C_2H_4 were measured. Figure 8d shows an apparent and new stretching bands at 3050–2850 and 1646 cm^{-1} that belong to C_3H_6 in C_3H_6-loaded MAC-4.[60] Besides, tiny changes at 1558 and 1537 cm^{-1} were observed, suggesting that C_3H_6 molecule formed the interactions with triazole rings (Figure S47).[61] Similarly, when C_2H_6 was loaded into MAC-4, characteristic peaks (2980 cm^{-1}) assigned to fundamental $\nu(CH_3)$ stretches of C_2H_6 molecule appeared (Figure 8e).[26,58] Meanwhile, the tiny changes at 1553 and 1538 cm^{-1} were also observed, indicating that C_2H_6 had multiple interactions with triazole rings (Figure S48). In contrast, no distinct peak change for C_2H_4-loaded MAC-4 was observed, which could be attributed to the weak interactions between C_2H_4 and the framework (Figure 8f). These IR spectroscopies qualitatively and partly supported the simulated results.

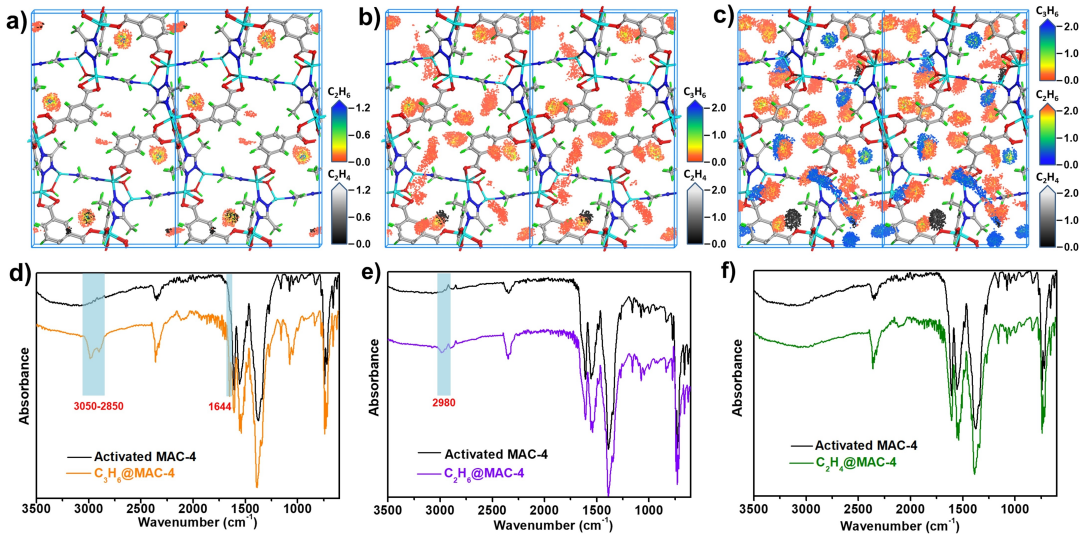

Figure 8. Simulated density distributions in MAC-4 for C_2H_6/C_2H_4 (a), C_2H_6/C_2H_4 (b), and $C_3H_6/C_2H_6/C_2H_4$ (c) mixtures; d-f) IR spectra of activated MAC-4, C_3H_6@MAC-4, C_2H_6@MAC-4 and C_2H_4@MAC-4.

Conclusions

In conclusion, we developed a deckgram-scale synthetic route of cheap and robust MOF MAC-4 with the goal of C_2H_4 purification from C_2H_6 and C_3H_6 mixtures. The non-polar pore surfaces with accessible O/N active sites endow the MOF with preferential adsorption for C_3H_6 and C_2H_6 over C_2H_4, leading to simultaneously high C_2H_6 and C_3H_6 uptakes and significant C_3H_6/C_2H_4 and C_2H_6/C_2H_4 selectivity. MAC-4 not only directly produces high-purity C_2H_4 ($\geq$ 99.9 %) from C_2H_6/C_2H_4 and C_3H_6/C_2H_4 mixtures, but also provides a high C_3H_6 ($\geq$ 99.5 %) recovery capacity through one adsorption-desorption procedure, which are highest in known materials. In addition, MAC-4 also realized one-step acquisition of C_2H_4 (99.9 %) and C_3H_6 (99.5 %) with the record productivities of 27.4 and 36.2 L kg^{-1} from $C_3H_6/C_2H_6/C_2H_4$ ternary mixtures. The comprehensive advantages on moisture stability, scalability, economic feasibility, separation performance, and reusability laid a solid foundation for MAC-4 to be applied in C_2H_4 purification and C_3H_6 recovery from the corresponding mixtures. This presentation would march an important step toward challenging C_2H_6/C_2H_4 and C_3H_6/C_2H_4 separation in applications and would facilitate the development of MOF-based adsorbents for new separation target as well.

Acknowledgements

This work is supported by National Natural Science Foundation of China (22371226 and 22371225) and Natural Science Basic Research Program of Shaanxi (2024JC-JCQN-18).

Conflict of Interest

The authors declare no conflict of interest.

Data Availability Statement

The data that support the findings of this study are available in the supplementary material of this article.

Keywords: metal–organic framework · scalable synthesis · gas adsorption and separation · ethylene purification · propylene recovery

[1] Y. Wang, T. Li, L. Li, R.-B. Lin, X. Jia, Z. Chang, H.-M. Wen, X.-M. Chen, J. Li, *Adv. Mater.* **2023**, *35*, 2207955.
[2] P. Zhang, L. Yang, X. Liu, J. Wang, X. Suo, L. Chen, X. Cui, H. Xing, *Nat. Commun.* **2022**, *13*, 4928.
[3] P. Hu, J. Hu, H. Liu, H. Wang, J. Zhou, R. Krishna, H. Ji, *ACS Cent. Sci.* **2022**, *8*, 1159–1168.
[4] Z. Di, C. Liu, J. Pang, S. Zou, Z. Ji, F. Hu, C. Chen, D. Yuan, M. Hong, M. Wu, *Angew. Chem. Int. Ed.* **2022**, *61*, e202210343.
[5] H. M. T. Galvis, J. H. Bitter, C. B. Khare, M. Ruitenbeek, A. I. Dugulan, K. P. De Jong, *Science* **2012**, *335*, 835–838.
[6] G.-D. Wang, Y.-Z. Li, W.-J. Shi, L. Hou, Y.-Y. Wang, Z. Zhu, *Angew. Chem. Int. Ed.* **2022**, *61*, e202205427.
[7] W. Fan, X. Wang, X. Zhang, X. Liu, Y. Wang, Z. Kang, F. Dai, B. Xu, R. Wang, D. Sun, *ACS Cent. Sci.* **2019**, *5*, 1261–1268.
[8] D. S. Sholl, R. P. Lively, *Nature* **2016**, *532*, 435–437.
[9] S. Jiang, J. Li, M. Feng, R. Chen, L. Guo, Q. Xu, L. Chen, F. Shen, Z. Zhang, Y. Yang, Q. Ren, Q. Yang, Z. Bao, *J. Mater. Chem. A* **2022**, *10*, 24127–24136.
[10] L. Yang, S. Qian, X. Wang, X. Cui, B. Chen, H. Xing, *Chem. Soc. Rev.* **2020**, *49*, 5359–5406.
[11] Y. Yang, L. Li, R.-B. Lin, Y. Ye, Z. Yao, L. Yang, F. Xiang, S. Chen, Z. Zhang, S. Xiang, B. Chen, *Nat. Chem.* **2021**, *13*, 933–939.
[12] K.-J. Chen, D. G. Madden, S. Mukherjee, T. Pham, K. A. Forrest, A. Kumar, B. Space, J. Kong, Q.-Y. Zhang, M, J. Zaworotkom, *Science* **2019**, *366*, 241–246.
[13] D.-D. Zhou, J.-P. Zhang, *Acc. Chem. Res.* **2022**, *55*, 2966–2977.
[14] G.-D. Wang, Y.-Z. Li, W.-J. Shi, B. Zhang, L. Hou, Y.-Y. Wang, *Sens. Actuators B* **2021**, *331*, 129377.
[15] X.-R. Tian, Z.-Y. Jiang, S.-L. Hou, H.-S. Hu, J. Li, B. Zhao, *Angew. Chem. Int. Ed.* **2023**, *62*, e202301764.
[16] Q. Yin, Z. Song, S. Yang, G.-D. Wang, Y. Sui, J. Qi, D. Zhao, L. Hou, Y.-Z. Li, *Chem. Sci.* **2023**,*14*, 5643–5649.
[17] G. Hu, Q. Liu, Y. Zhou, W. Yan, Y. Sun, S. Peng, C. Zhao, X. Zhou, H. Deng, *J. Am. Chem. Soc.* **2023**, *145*, 13181–13194.
[18] W. Yang, Q. Liu, J. Yang, J. Xian, Y. Li, G. Li, C.-Y. Su, *CCS Chem.* **2022**, *4*, 2276–2285.
[19] S.-Q. Yang, R. Krishna, H. Chen, L. Li, L. Zhou, Y.-F. An, F.-Y. Zhang, Q. Zhang, Y.-H. Zhang, W. Li, T.-L. Hu, X.-H. Bu, *J. Am. Chem. Soc.* **2023**, *145*, 13901–13911.
[20] C. Yu, Z. Guo, L. Yang, J. Cui, S. Chen, Y. Bo, X. Suo, Q. Gong, S. Zhang, X. Cui, S. He, H. Xing, *Angew. Chem. Int. Ed.* **2023**, *62*, e202218027.
[21] D. Liu, J. Pei, X. Zhang, X.-W Gu, H.-M. Wen, B. Chen, G. Qian, B. Li, *Angew. Chem. Int. Ed.* **2023**, *62*, e202218590.
[22] Z. Zhang, Z. Deng, H. A. Evans, D. Mullangi, C. Kang, S. B. Peh, Y. Wang, C. M. Brown, J. Wang, P. Canepa, A. K. Cheetham, D. Zhao, *J. Am. Chem. Soc.* **2023**, *145*, 11643–11649.
[23] Y. Jiang, Y. Hu, B. Luan, L. Wang, R. Krishna, H. Ni, X. Hu, Y. Zhang, *Nat. Commun.* **2023**, *14*, 401.
[24] H. Zeng, M. Xie, T. Wang, R.-J. Wei, X.-J. Xie, Y. Zhao, W. Lu, D. Li, *Nature* **2021**, *595*, 542–548.
[25] Y. Ye, Y. Xie, Y. Shi, L. Gong, J. Phipps, A. M. Al-Enizi, A. Nafady, B. Chen, S. Ma, *Angew. Chem. Int. Ed.* **2023**, *62*, e202302564.
[26] S. Geng, E. Lin, X. Li, W. Liu, T. Wang, Z. Wang, D. Sensharma, S. Darwish, Y. H. Andaloussi, T. Pham, P. Cheng, M. J. Zaworotko, Y. Chen, Z. Zhang, *J. Am. Chem. Soc.* **2021**, *143*, 8654–8660.
[27] S.-Q. Yang, T.-L. Hu, *Coord. Chem. Rev.* **2022**, *468*, 214628.
[28] D. Lv, P. Zhou, J. Xu, S. Tu, F. Xu, J. Yan, H. Xi, W. Yuan, Q. Fu, X. Chen, Q. Xia, *Chem. Eng. J.* **2022**, *431*, 133208.
[29] Q. Ding, Z. Zhang, Y. Liu, K. Chai, R. Krishna, S. Zhang, *Angew. Chem. Int. Ed.* **2022**, *61*, e202208134.
[30] H.-G. Hao, Y.-F. Zhao, D.-M. Chen, J.-M. Yu, K. Tan, S. Ma, Y. Chabal, Z.-M. Zhang, J.-M. Dou, Z.-H. Xiao, G. Day, H.-C. Zhou, T.-B. Lu, *Angew. Chem. Int. Ed.* **2018**, *57*, 16067–16071.
[31] L. Zhang, L.-N. Ma, G.-D. Wang, L. Hou, Z. Zhu, Y.-Y. Wang, *J. Mater. Chem. A* **2023**, *11*, 2343–2348.
[32] G.-D. Wang, Y.-Z. Li, W.-J. Shi, L. Hou, Y.-Y. Wang, Z. Zhu, *Angew. Chem. Int. Ed.* **2023**, *62*, e202311654.
[33] M. Kang, D. W. Kang, J. H. Choe, H. Kim, D. W. Kim, H. Park, C. S. Hong, *Chem. Mater.* **2021**, *33*, 6193–6199.
[34] Y.-Z. Li, G.-D. Wang, R. Krishna, Q. Yin, D. Zhao, J. Qi, Y. Sui, L. Hou, *Chem. Eng. J.* **2023**, *466*, 143056.

[35] G.-D. Wang, R. Krishna, Y.-Z. Li, Y.-Y. Ma, L. Hou, Y.-Y. Wang, Z. Zhu, *ACS Materials Lett.* **2023**, *5*, 1091–1099.
[36] Y. Ling, F. Yang, M. Deng, Z. Chen, X. Liu, L. Weng, Y. Zhou, *Dalton Trans.* **2012**, *41*, 4007–4011.
[37] O. T. Qazvini, R. Babarao, Z.-L. Shi, Y.-B. Zhang, S. G. Telfer, *J. Am. Chem. Soc.* **2019**, *141*, 5014–5020.
[38] Z. Xu, X. Xiong, J. Xiong, R. Krishna, L. Li, Y. Fan, F. Luo, B. Chen, *Nat. Commun.* **2020**, *11*, 3163.
[39] F. Jin, E. Lin, T. Wang, S. Geng, T. Wang, W. Liu, F. Xiong, Z. Wang, Y. Chen, P. Cheng, Z. Zhang, *J. Am. Chem. Soc.* **2022**, *144*, 5643–5652.
[40] L. Li, R.-B. Lin, R. Krishna, H. Li, S. Xiang, H. Wu, J. Li, W. Zhou, B. Chen, *Science* **2018**, *362*, 443–446.
[41] P.-Q. Liao, W.-X. Zhang, J.-P. Zhang, X.-M. Chen, *Nat. Commun.* **2015**, *6*, 8697.
[42] H. Yang, Y. Wang, R. Krishna, X. Jia, Y. Wang, A. N. Hong, C. Dang, H. E. Castillo, X. Bu, P. Feng, *J. Am. Chem. Soc.* **2020**, *142*, 2222–2227.
[43] J. Pei, J.-X. Wang, K. Shao, Y. Yang, Y. Cui, H. Wu, W. Zhou, B. Li, G. Qian, *J. Mater. Chem. A* **2020**, *8*, 3613–3620.
[44] Y.-P. Li, Y.-N. Zhao, S.-N. Li, D.-Q. Yuan, Y.-C. Jiang, X. Bu, M.-C. Hu, Q.-G. Zhai, *Adv. Sci.* **2021**, *8*, 2003141.
[45] K. Su, W. Wang, S. Du, C. Ji, D. Yuan, *Nat. Commun.* **2021**, *12*, 3703.
[46] X. Liu, C. Hao, J. Li, Y. Wang, Y. Hou, X. Li, L. Zhao, H. Zhu, W. Guo, *Inorg. Chem. Front.* **2018**, *5*, 2898–2905.
[47] R. Krishna, *RSC Adv.* **2017**, *7*, 35724–35737.
[48] R. Krishna, *ACS Omega* **2020**, *5*, 16987–17004.
[49] G.-D. Wang, R. Krishna, Y.-Z. Li, W.-J. Shi, L. Hou, Y.-Y. Wang, Z. Zhu, *Angew. Chem. Int. Ed.* **2022**, *61*. e202213015.
[50] Y. Xiao, A. N. Hong, Y. Chen, H. Yang, Y. Wang, X. Bu, P. Feng, *Small* **2023**, *19*, 2205119.
[51] X.-M. Liu, L.-H. Xie, Y. Wu, *Materials* **2023**, *16*, 154.
[52] R. Krishna, *Microporous Mesoporous Mater.* **2014**, *185*, 30–50.
[53] R. Krishna, *RSC Adv.* **2015**, *5*, 52269–52295.
[54] R. Krishna, *Sep. Purif. Technol.* **2018**, *194*, 281–300.
[55] R. Krishna, *Precision Chemistry* **2023**, *1*, 83–93.
[56] H. Zeng, X.-J. Xie, M. Xie, Y.-L. Huang, D. Luo, T. Wang, Y. Zhao, W. Lu, D. Li, *J. Am. Chem. Soc.* **2019**, *141*, 20390–20396.
[57] X. Zhang, L. Li, J.-X. Wang, H.-M. Wen, R. Krishna, H. Wu, W. Zhou, Z.-N. Chen, B. Li, G. Qian, B. Chen, *J. Am. Chem. Soc.* **2020**, *142*, 633–640.
[58] W. Liu, S. Geng, N. Li, S. Wang, S. Jia, F. Jin, T. Wang, K. A. Forrest, T. Pham, P. Cheng, Y. Chen, J.-G. Ma, Z. Zhang, *Angew. Chem. Int. Ed.* **2023**, *62*, e202217662.
[59] Y. Zhou, C. Chen, R. Krishna, Z. Ji, D. Yuan, M. Wu, *Angew. Chem. Int. Ed.* **2023**, *62*, e202305041.
[60] Y. Xie, Y. Shi, E. M. C. Morales, A. E. Karch, B. Wang, H. Arman, K. Tan, B. Chen, *J. Am. Chem. Soc.* **2023**, *145*, 2386–2394.
[61] H.-M. Wen, C. Yu, M. Liu, C. Lin, B. Zhao, H. Wu, W. Zhou, B. Chen, J. Hu, *Angew. Chem. Int. Ed.* **2023**, *62*, e202309108.

Manuscript received: December 24, 2023
Accepted manuscript online: February 18, 2024
Version of record online: March 1, 2024

Angewandte Chemie
Eine Zeitschrift der Gesellschaft Deutscher Chemiker

Supporting Information

Scalable Synthesis of Robust MOF for Challenging Ethylene Purification and Propylene Recovery with Record Productivity

G.-D. Wang, Y.-Z. Li, R. Krishna, W.-Y. Zhang, L. Hou, Y.-Y. Wang, Z. Zhu*

Supporting Information

69451 Weinheim, Germany

Scalable Synthesis of Robust MOF for Challenging Ethylene Purification and Propylene Recovery with Record Productivity

Gang-Ding Wang,[+,a] Yong-Zhi Li,[+,a,c] Rajamani Krishna,[b] Wen-Yan Zhang,[a] Lei Hou,*[a] Yao-Yu Wang,[a] and Zhonghua Zhu[d]

Abstract: Ethylene (C_2H_4) purification and propylene (C_3H_6) recovery are highly relevant in polymer synthesis, yet developing physisorbents for these industrial separation faces the challenges of merging easy scalability, economic feasibility, high moisture stability with great separation efficiency. Herein, we reported a robust and scalable MOF (MAC-4) for simultaneous recovery of C_3H_6 and C_2H_4. Through creating nonpolar pores decorated by accessible N/O sites, MAC-4 displays top-tier uptakes and selectivities for C_2H_6 and C_3H_6 over C_2H_4 at ambient conditions. Molecular modelling combined with infrared spectroscopy revealed that C_2H_6 and C_3H_6 molecules were trapped in the framework with stronger contacts relative to C_2H_4. Breakthrough experiments demonstrated exceptional separation performance for binary C_2H_6/C_2H_4 and C_3H_6/C_2H_4 as well as ternary $C_3H_6/C_2H_6/C_2H_4$ mixtures, simultaneously affording record productivities of 27.4 and 36.2 L kg^{-1} for high-purity C_2H_4 (≥ 99.9 %) and C_3H_6 (≥ 99.5 %). MAC-4 was facilely prepared at deckgram-scale under reflux condition within 3 hours, making it as a smart MOF to address challenging gas separations.

DOI: 10.1002/anie.2023XXXXX

Table of Contents

Materials and general methods

The reagents were purchased commercially. Thermalgravimetric analyses (TGA) were tested in a nitrogen stream using a Netzsch TG209F3 equipment (10 °C min^{-1}). Powder X-ray diffraction (PXRD) data were recorded on a Bruker D8 ADVANCE X-ray powder diffractometer (Cu Kα, λ = 1.5418 Å). Water sorption was collected by Quantachrome Vstar vapor adsorption equipment. Sorption measurements were performed with an automatic volumetric sorption apparatus (Micrometrics TriStar II 3020), in which the sample was activated at 393 K under vacuum for 4 hours. Breakthrough experiments were performed on a Quantachrome dynaSorb BT equipment. All the IR spectroscopic data are recorded in INVENIO S ATR-FTIR spectrometer.

Synthesis of MAC-4

Solvothermal synthesis of MAC-4 crystals

MAC-4 crystal was synthesized according to a previously published report.[1] The solution of 0.3 mmol 3,5-dimethyl-1,2,4-triazolate (Hdmtrz) (0.028 g) and 0.3 mmol isophthalic acid (H_2ipa) (0.049 g) in 5 mL of N, N-dimethylformamide (DMF) was added to the solution 5 mL DMF containing 0.45 mmol $Zn(OAc)_2{\cdot}2H_2O$ (0.089 g). The next solvothermal reactions heated at 140 °C for 3 days yielded MAC-4 crystals.

Scale-up synthesis of MAC-4 microcrystalline

The deckgram-scale synthesis of MAC-4 was performed under reflux conditions. 54 mmol $Zn(OAc)_2{\cdot}2H_2O$ (10.68 g), 36 mmol Hdmtrz (3.36 g), 36 mmol H_2ipa (5.88 g) were stirred in DMF (300 mL) until it was fully dissolved (Figure 1a). Then the solutions were refluxed at 120 °C for 3 hours. The white microcrystalline of MAC-4 was collected through filtration, and then dried in air environment (Yield: 10.2 g, 77.7% based on Zn^{2+} ions) (Figure 1b). Note, the DMF can be recovered by filtrating for continued synthesis of MAC-4 at least three cycles.

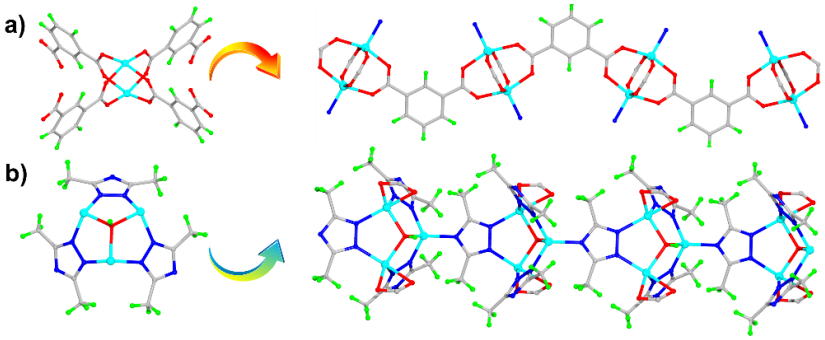

Figure S1. a) 1D chains composed of $[Zn_2(COO)_4]$ SBUs; b) 1D chains composed of $[Zn_3(OH)(dmtrz)_3]$ SBUs.

Powder X-ray diffraction (PXRD)

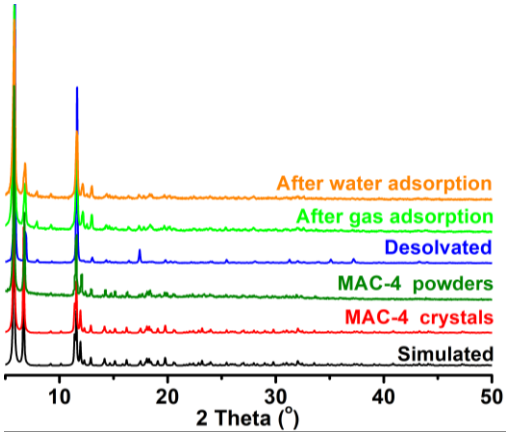

Figure S2. PXRD patterns of MAC-4.

Thermogravimetric analysis (TGA)

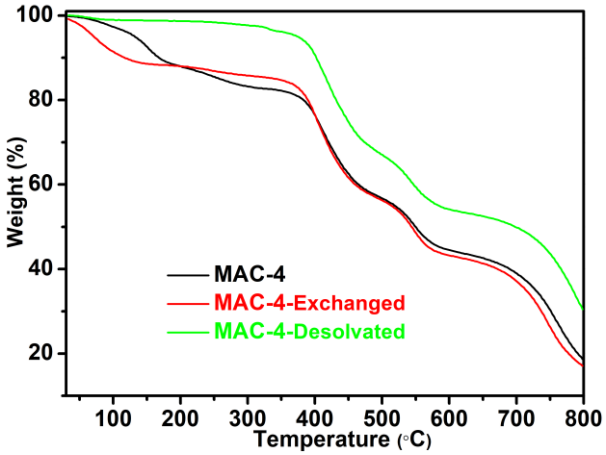

Figure S3. TGA curves of as-synthesized, exchanged, and desolvated samples of MAC-4.

N_2 adsorption isotherms

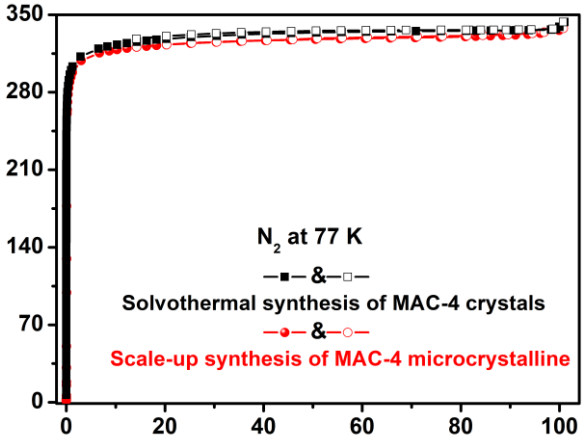

Figure S4. Comparison of N_2 adsorption isotherms (77 K) of MAC-4 synthesized by different methods.

Water adsorption isotherms

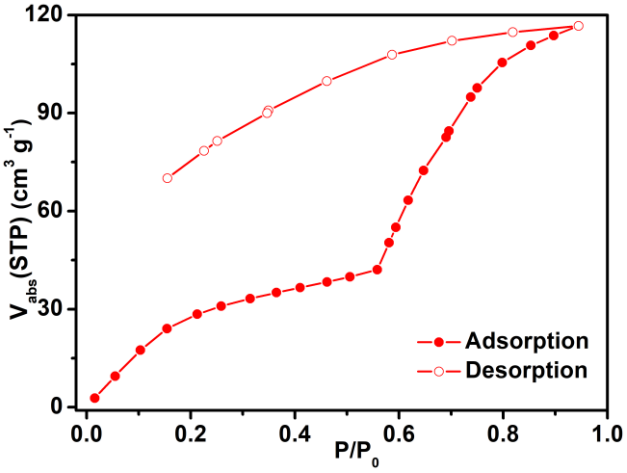

Figure S5. Water vapor adsorption and desorption isotherm of MAC-4 at 298 K.

Gas adsorption isotherms

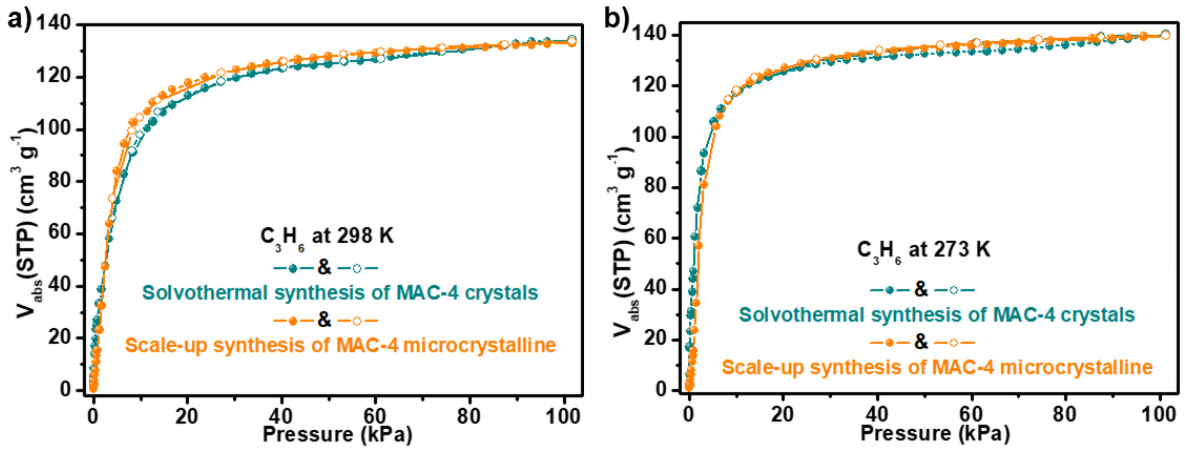

Figure S6. The comparison of adsorption isotherm curves of solvothermal synthesis of MAC-4 crystals samples and scale-up synthesis of MAC-4 microcrystalline samples for C_3H_6 at 298 K a); and 273 K b).

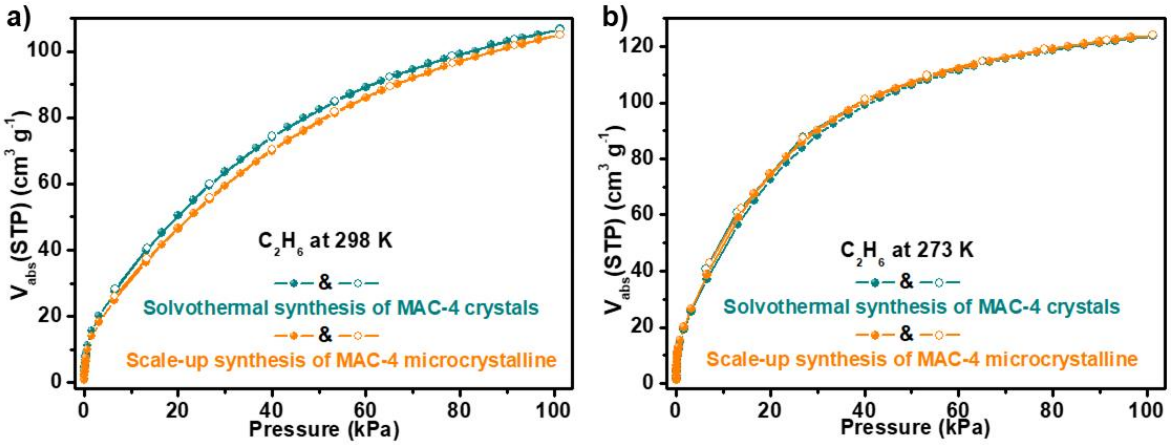

Figure S7. The comparison of adsorption isotherm curves of solvothermal synthesis of MAC-4 crystals samples and scale-up synthesis of MAC-4 microcrystalline samples for C_2H_6 at 298 K a); and 273 K b).

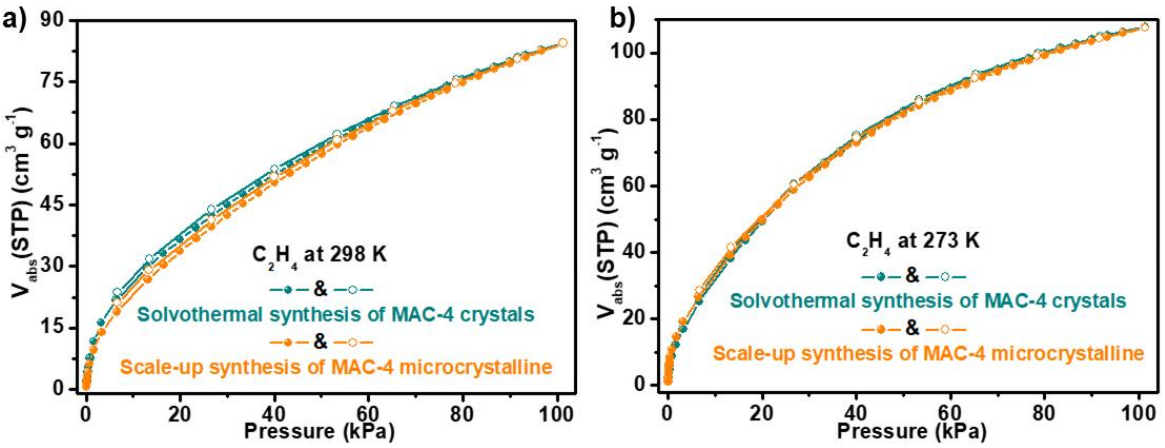

Figure S8. The comparison of adsorption isotherm curves of solvothermal synthesis of MAC-4 crystals samples and scale-up synthesis of MAC-4 microcrystalline samples for C_2H_4 at 298 K a); and 273 K b).

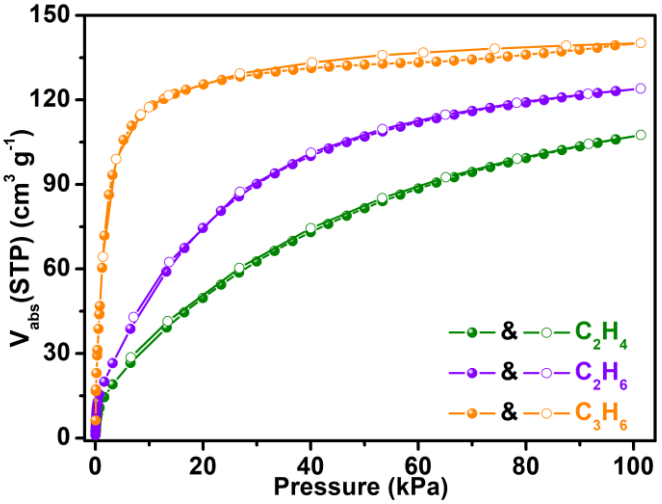

Figure S9. C_3H_6, C_2H_4 and C_2H_6 adsorption isotherms of MAC-4 at 273 K.

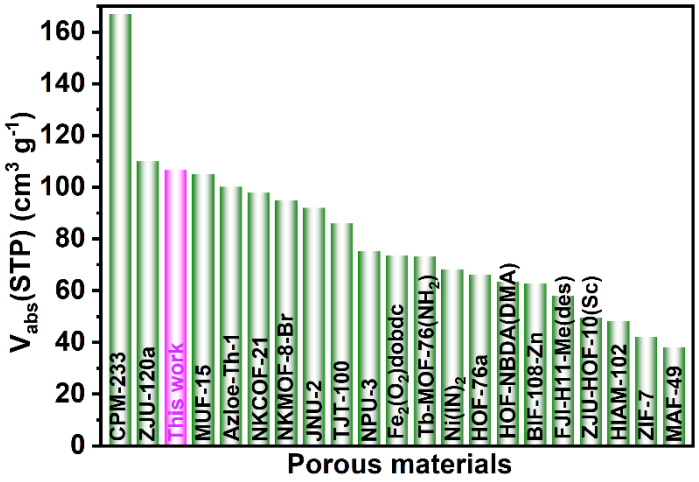

Figure S10. Comparisons of C_2H_6 uptakes in MAC-4 and leading materials at 298 K.

Fitting adsorption heat of pure component isotherms

The unary isotherms for C_3H_6, C_2H_6, and C_2H_4, measured at two different temperatures 273 K, and 298 K in MAC-4 were fitted with excellent accuracy using the dual-site Langmuir model, where we distinguish two distinct adsorption sites A and B:

$$q=\frac{q_{sat,A}b_Ap}{1+b_Ap}+\frac{q_{sat,B}b_Bp}{1+b_Bp} \quad \text{(S1)}$$

In eq), the Langmuir parameters b_A, b_B are both temperature dependent

$$b_A=b_{A0}\,exp\left(\frac{E_A}{RT}\right);\quad b_b=b_{B0}\,exp\left(\frac{E_B}{RT}\right) \quad \text{(S2)}$$

In eq (S2), E_A, E_B are the energy parameters associated with sites A, and B, respectively.

The unary isotherm fit parameters are provided in **Fehler! Verweisquelle konnte nicht gefunden werden.**.

The isosteric heat of adsorption, Q_{st}, is defined as

$$Q_{st}=-RT^2\left(\frac{\partial \ln p}{\partial T}\right)_q \quad \text{(S3)}$$

where, the derivative in the right member of eq (S3) is determined at constant adsorbate loading, q. the derivative was determined by analytic differentiation of the combination of eq), eq (S2), and eq (S3).

Table S1. Dual-site Langmuir fits for C_3H_6, C_2H_6, and C_2H_4 in MAC-4.

	Site A			Site B		
	$q_{A,sat}$ mol/kg	b_{A0} Pa^{-1}	E_A kJ mol^{-1}	$q_{B,sat}$ mol/kg	b_{B0} Pa^{-1}	E_B kJ mol^{-1}
C_3H_6	5.4	4.253E-10	31.7	0.7	4.062E-07	24
C_2H_6	6.3	8.897E-09	19	0.6	2.389E-07	23
C_2H_4	6.8	5.481E-09	18	0.7	1.012E-06	17

Gas adsorption cycles

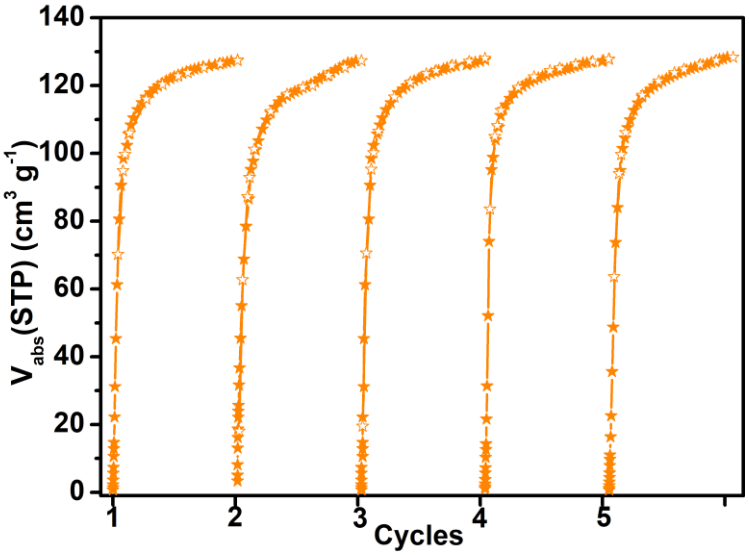

Figure S11. Repetitive C_3H_6 adsorption curves at 298 K.

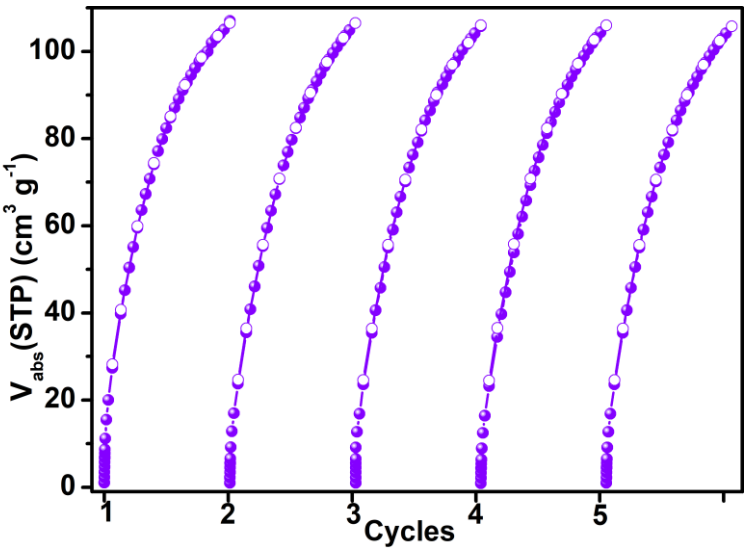

Figure S12. Repetitive C_2H_6 adsorption curves at 298 K.

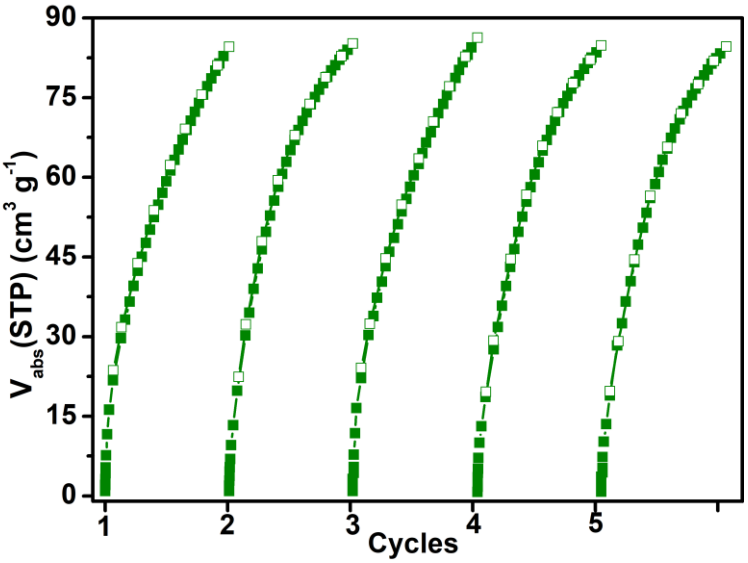

Figure S13. Repetitive C_2H_4 adsorption curves at 298 K.

Estimation of production cost of MAC-4

Table S2. The raw material cost of various adsorbents.

Material	Price ($ g^{-1})	Source
$Zn(OAc)_2 \cdot 2H_2O$	0.003 $ g^{-1}	Greagent
Hdmtrz	2.469 $ g^{-1}	Adamas
H_2IPA	0.007 $ g^{-1}	Adamas
DMF	0.018 $ mL^{-1}	Sigma-Aldrich
MAC-4	1.349 $ g^{-1}	Synthesis

Note: Material cost was calculated by using the required amounts of metal salts and organic ligands precursor. Additionally, the cost of the operation and utility cost for hydrothermal reaction, filtrate, and drying, etc. are not considered.

Gas selectivity prediction via IAST

The experimental isotherm data for pure C_3H_6, C_2H_4 and C_2H_6 were fitted using a dual-site Langmuir-Freundlich (L-F) model:

$$q = \frac{a_1 * b_1 * P^{c_1}}{1 + b_1 * P^{c_1}} + \frac{a_2 * b_2 * P^{c_2}}{1 + b_2 * P^{c_2}}$$

Where *q* and *p* are adsorbed amounts and the pressure of component i, respectively.

The adsorption selectivities for binary mixtures defined by

$$S_{i/j} = \frac{x_i * y_j}{x_j * y_i}$$

wererespectively calculated using the Ideal Adsorption Solution Theory (IAST). Where x_i is the mole fraction of component *i* in the adsorbed phase and y_i is the mole fraction of component i in the bulk.

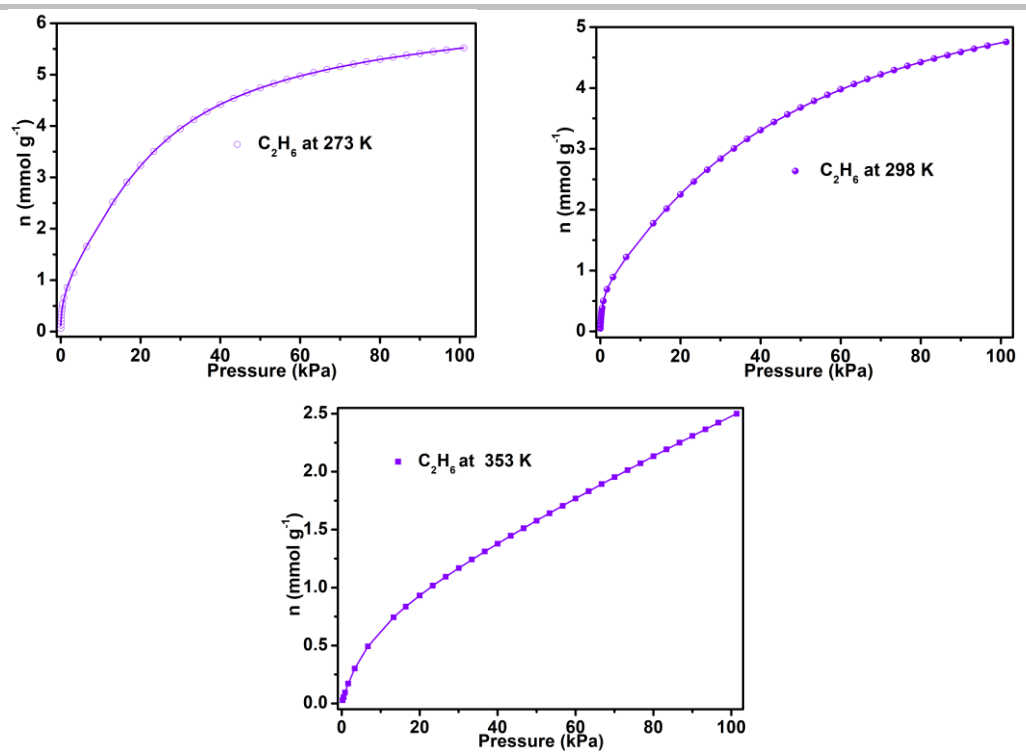

Figure S14. C_2H_6 adsorption isotherms of MAC-4 with fitted by dual L-F model, 273 K: a1 = 2.44243, b1 = 0.00296, c1 = 1.89301, a2 = 5.86278, b2 = 0.13443, c2 = 0.47539, Chi^2 = 0.00041, R^2 = 0.99992; 298 K: a1 = 5.58896, b1 = 0.01072, c1 = 1.18007, a2 = 0.77584, b2 = 1.89883, c2 = 0.97692, Chi^2 = 0.00002, R^2 = 0.99999; 353 K: a1 = 11.54749, b1 = 0.00088, c1 = 1.14146, a2 = 0.87088, b2 = 0.12614, c2 = 1.00959, Chi^2 = 6.818E-7, R^2 = 1.

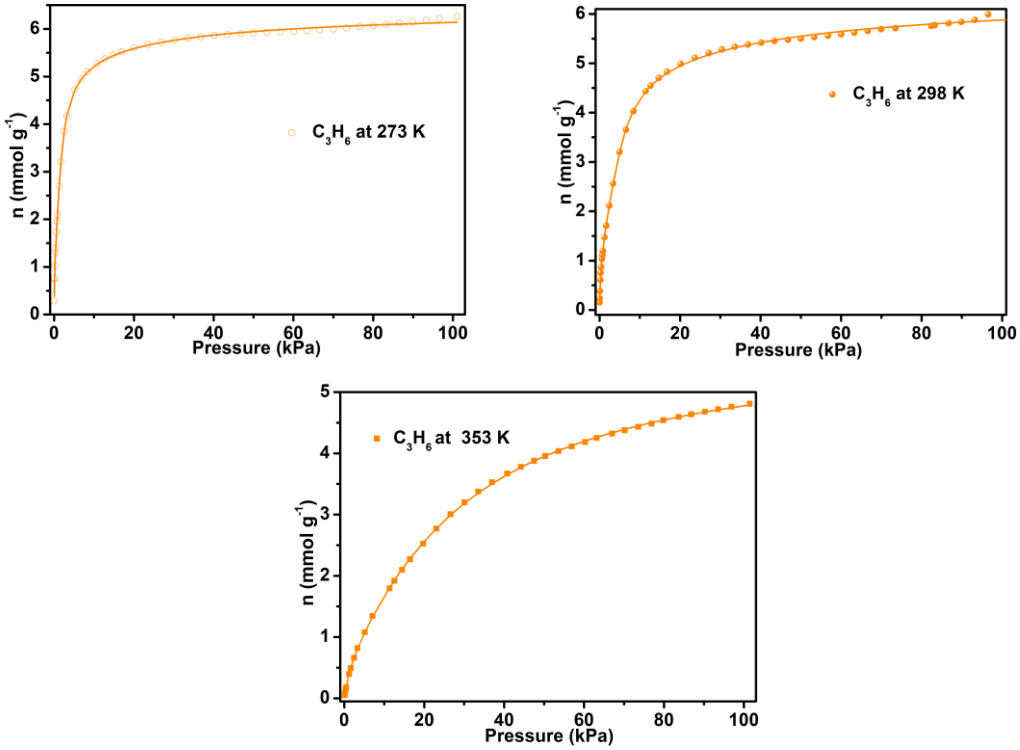

Figure S15. C_3H_6 adsorption isotherms of MAC-4 with fitted by dual L-F model, 273 K: a1 = 4.63475, b1 = 0.66052, c1 = 0.56825, a2 = 1.96456, b2 = 0.34334, c2 = 2.14875, Chi^2 = 0.00154, R^2 = 0.99962; 298 K: a1 = 5.36762, b1 = 0.32974, c1 = 0.64812, a2 = 1.22382, b2 = 0.0082, c2 = 2.97596, Chi^2 = 0.00201, R^2 = 0.99957; 353 K: a1 = 5.06649, b1 = 0.01649, c1 = 1.20353, a2 = 0.68958, b2 = 0.60603, c2 = 1.08723, Chi^2 = 0.00018, R^2 = 0.99994.

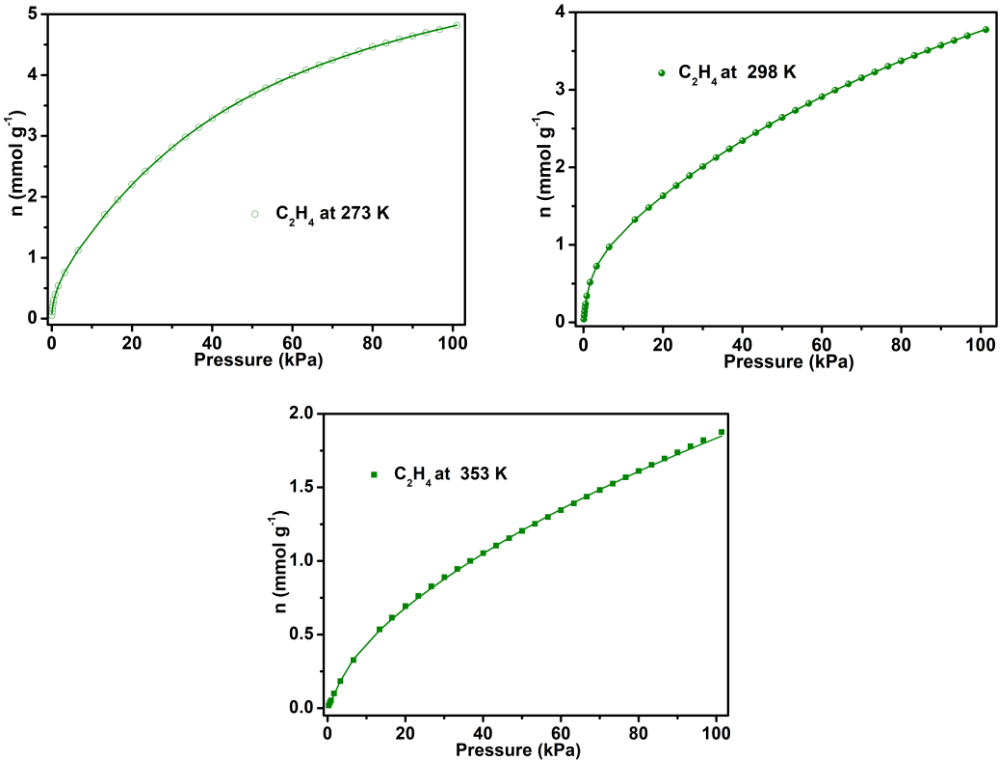

Figure S16. C_2H_4 adsorption isotherms of MAC-4 with fitted by dual L-F model, 273 K: a1 = 9.43954, b1 = 0.04569, c1 = 0.52526, a2 = 1.87921, b2 = 0.002, c2 = 1.73163, Chi^2 = 0.00008, R^2 = 0.99998; 298 K: a1 = 6.88414, b1 = 0.00606, c1 = 1.04001, a2 = 0.87108, b2 = 0.64858, c2 = 0.97491, Chi^2 = 3.3222E-6, R^2 =1; 353 K: a1 = 6.50703, b1 = 0.00649, c1 = 0.8607, a2 = 0.17791, b2 = 0.07126, c2 = 1.81603, Chi^2 = 0.00011, R^2 = 0.99973.

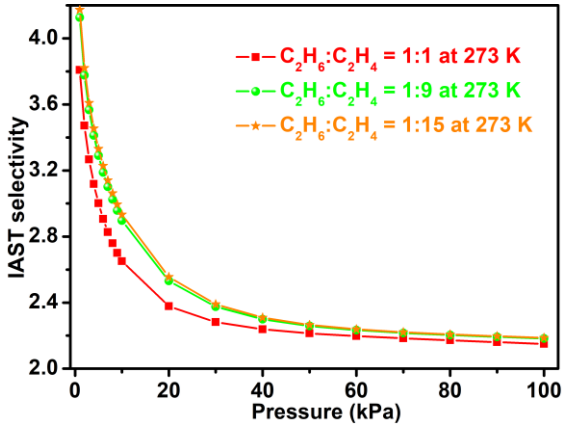

Figure S17. IAST selectivity curves of MAC-4 for C_2H_6/C_2H_4 at 273 K.

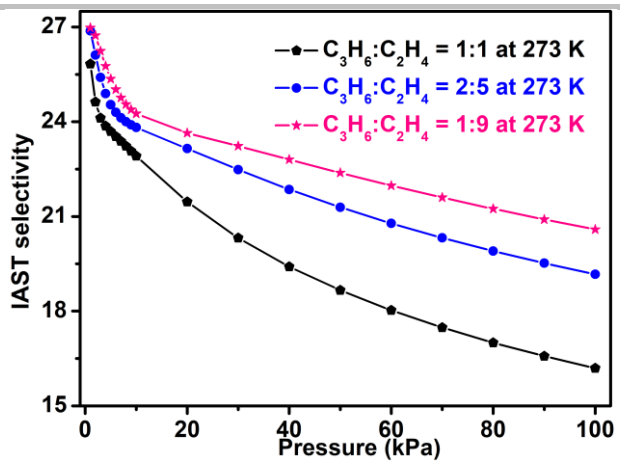

Figure S18. IAST selectivity curves of MAC-4 for C_3H_6/C_2H_4 at 273 K.

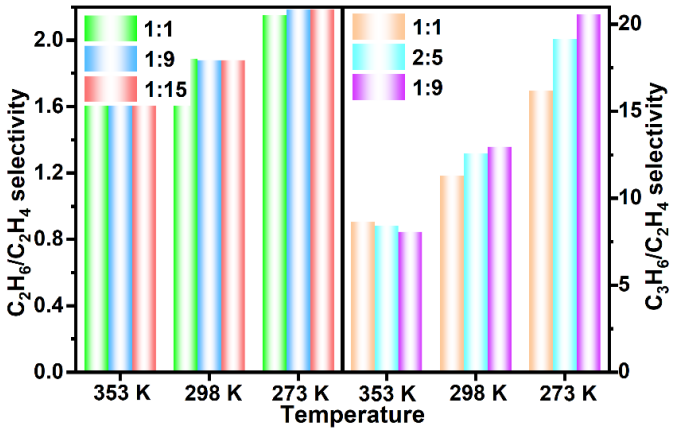

Figure S19. IAST selectivity values of MAC-4 for C_2H_6/C_2H_4 and C_3H_6/C_2H_4 at 353, 298, and 273 K.

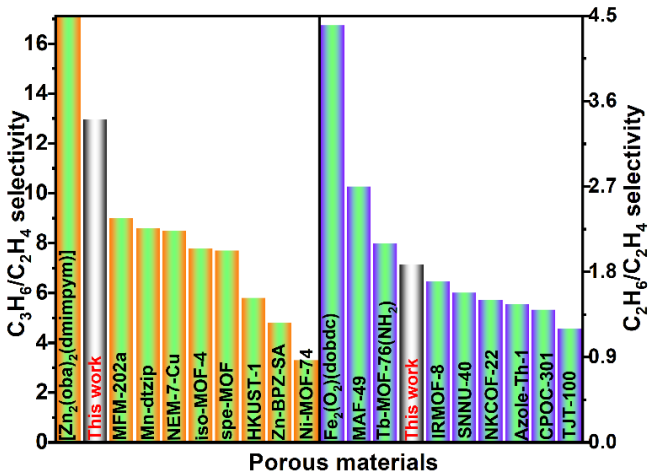

Figure S20. Comparison of C_3H_6/C_2H_4 (left) and C_2H_6/C_2H_4 (right) selectivities in MAC-4 and some benchmark adsorbents at 298 K.

Separation potential

For separation of binary 50/50 $C_2H_6(1)/C_2H_4(2)$, 50/50 $C_3H_6(1)/C_2H_4(2)$ mixtures, the maximum productivity of purified C_2H_4 that is theoretically achievable in a fixed bed adsorber is determined by the metric defined by Krishna[2,3] as the separation potential, ΔQ, derived on the basis of the shock wave model

For 50/50 $C_2H_6(1)/C_2H_4(2)$ mixtures: $\Delta Q=(q_{C2H6})\frac{50}{50}-q_{C2H4}$; For 50/50 $C_3H_6(1)/C_2H_4(2)$ mixtures: $\Delta Q=(q_{C3H6})\frac{50}{50}-q_{C2H4}$

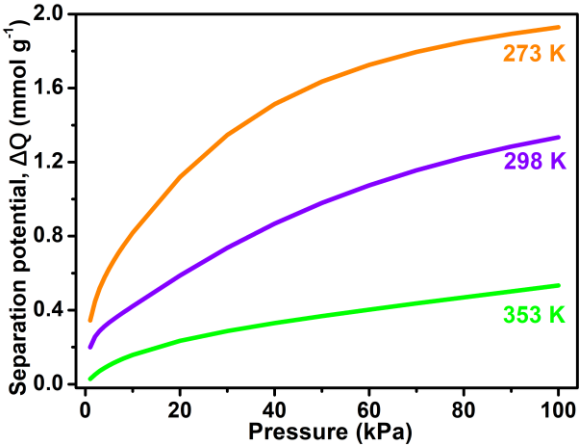

Figure S21. Separation potential of MAC-4 for C_2H_6/C_2H_4 mixtures at 273, 298, and 353K.

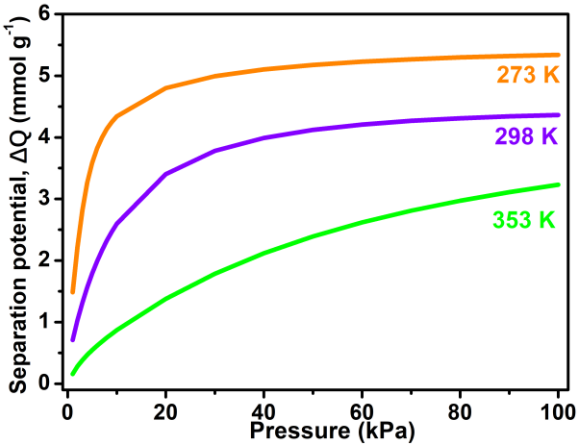

Figure S22. Separation potential of MAC-4 for C_3H_6/C_2H_4 mixtures at 273, 298, and 353K.

GCMC simulation

Grand canonical Monte Carlo (GCMC) simulations were performed for the gas adsorption in the framework by the Sorption module of Material Studio (Accelrys. Materials Studio Getting Started). The framework was considered to be rigid, and the optimized gas molecules were used. The partial charges for atoms of the framework were derived from QEq method and QEq neutral 1.0 parameter. One unit cell was used during the simulations. The interaction energies between the gas molecules and framework were computed through the Coulomb and Lennard-Jones 6-12 (LJ) potentials. All parameters for the atoms were modeled with the universal force field (UFF) embedded in the MS modeling package. A cutoff distance of 12.5 Å was used for LJ interactions, and the Coulombic interactions were calculated by using Ewald summation. For each run, the 3×10^6 maximum loading steps, 3×10^6 production steps were employed. The binding energy was calculated by following equation: $E_{bind} = E_{framework+gas} - E_{framework} - E_{gas}$, in which $E_{framework+gas}$ is the total energy of the framework and the adsorbed gas molecule, $E_{framework}$ and E_{gas} are the energies of the framework and gas molecule. The exchange-correlation functional used in calculations was in the framework of the generalized gradient approximation (GGA) proposed by Perdew, Burke and Ernzerhof (PBE). DNP basis set was used to describe the atomic orbital. The SCF convergence was set to 1×10^{-6}.

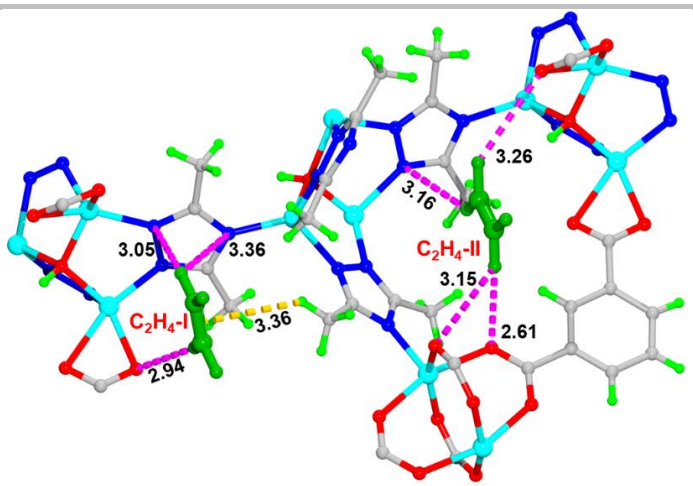

Figure S23. Adsorption sites for C_2H_4-I and C_2H_4-II at 298 K under 100 kPa (H, green; Zn, turquiose; C, gray; O, red; N, blue).

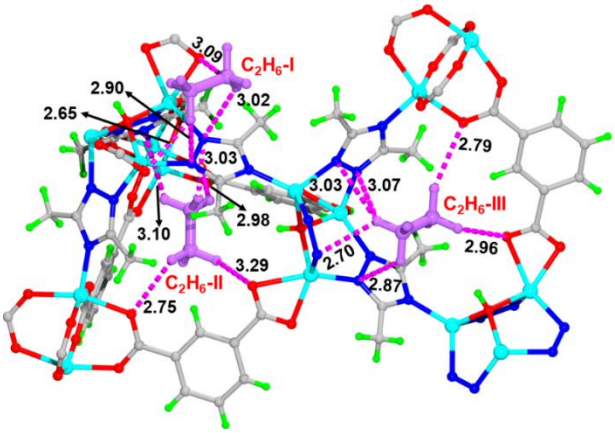

Figure S24. Adsorption sites for C_2H_6-I, C_2H_6-II and C_2H_6-III at 298 K under 100 kPa (H, green; Zn, turquiose; C, gray; O, red; N, blue).

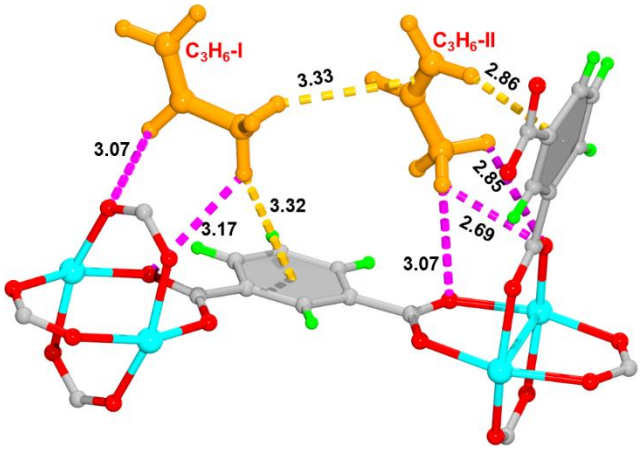

Figure S26. Adsorption sites for C_3H_6-I and C_2H_6-II at 298 K under 100 kPa (H, green; Zn, turquiose; C, gray; O, red; N, blue).

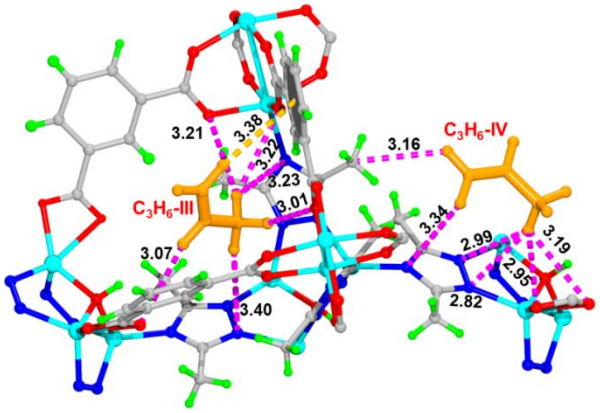

Figure S26. Adsorption sites for C_3H_6-I and C_2H_6-IV at 298 K under 100 kPa (H, green; Zn, turquiose; C, gray; O, red; N, blue).

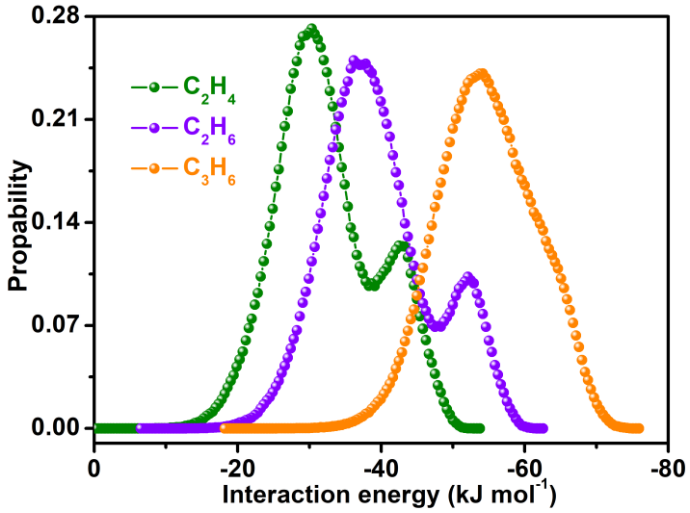

Figure S27. Interaction energy distribution of C_2H_4, C_2H_6, and C_3H_6 in the MAC-4.

Breakthrough experiments

The breakthrough experiments were performed on the Quantachrome dynaSorb BT equipments at 273, 298 and 353 K and 100 kPa with Ar as the carrier gas. The activated MAC-4 (about 0.88 g) was filled into a packed column of ϕ 4.2 mm × 80 mm, and then the packed column was washed with Ar at a rate of 7 mL min^{-1} at 343 K for 50 minutes to further activate the samples. Between two breakthrough experiments, the adsorbent was regenerated by Ar flow of 7 mL min^{-1} for 35 min at 343 K to guarantee a complete removal of the adsorbed gas.

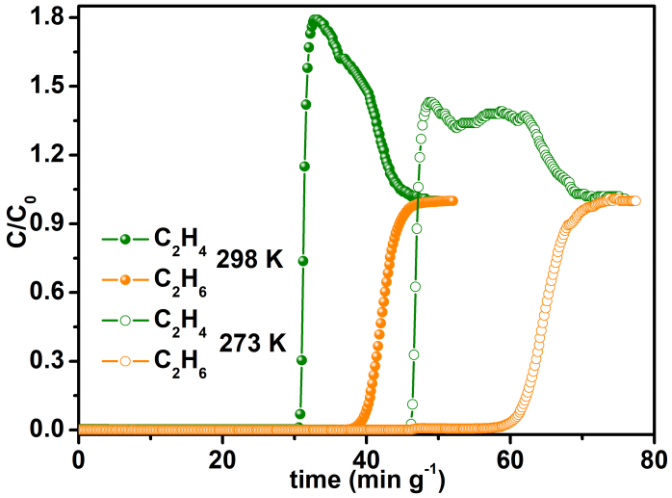

Figure S28. Breakthrough curves of MAC-4 for equimolar C_2H_6/C_2H_4 (10/10, v/v) mixtures at 298 and 273 K with Ar as the carrier gas (80%, vol%).

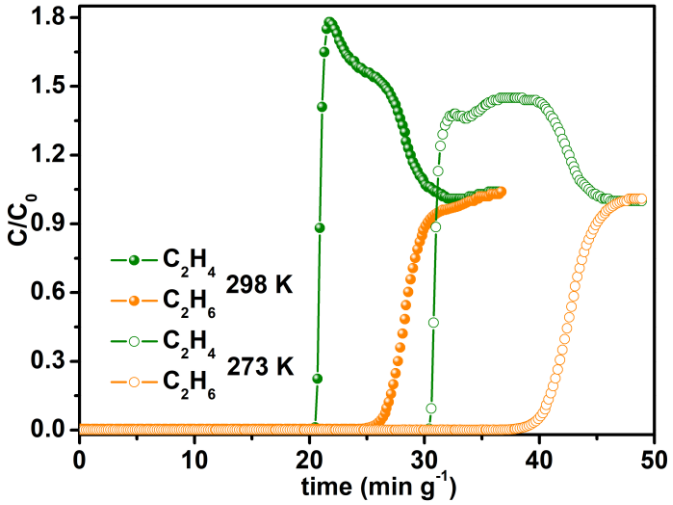

Figure S29. Breakthrough curves of MAC-4 for equimolar C_2H_6/C_2H_4 (20/20, v/v) mixtures at 298 and 273 K with Ar as the carrier gas (60%, vol%).

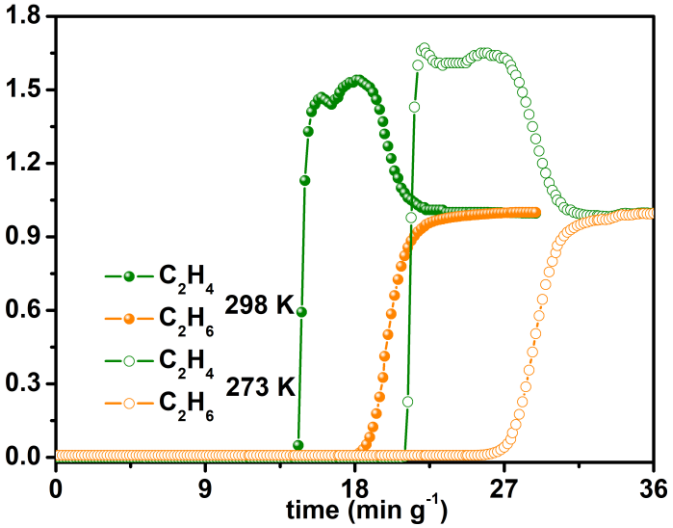

Figure S30. Breakthrough curves of MAC-4 for equimolar C_2H_6/C_2H_4 (30/30, v/v) mixtures at 298 and 273 K with Ar as the carrier gas (40%, vol%).

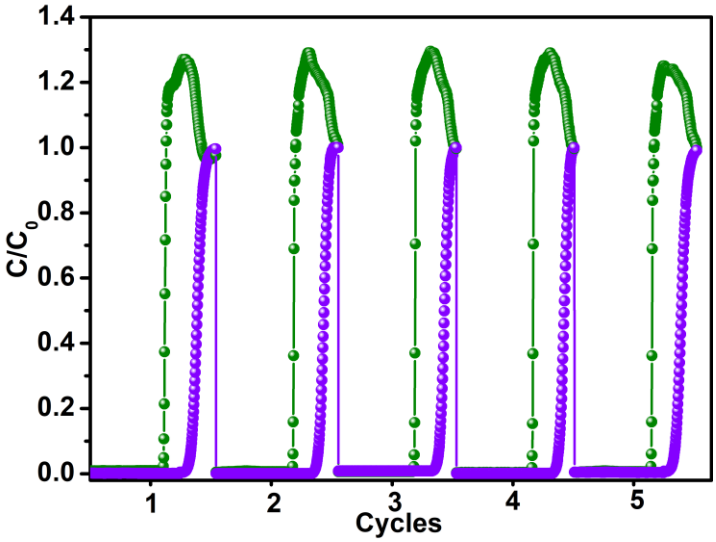

Figure S31. Breakthrough cycles of MAC-4 for C_2H_6/C_2H_4 mixtures at 298 K.

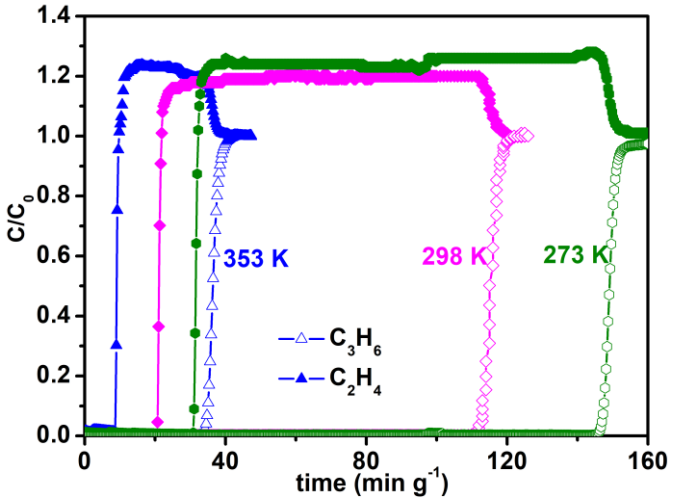

Figure S32. Breakthrough curves for C_3H_6/C_2H_4 (v/v, 10/25) mixtures at 353, 298 and 273 K.

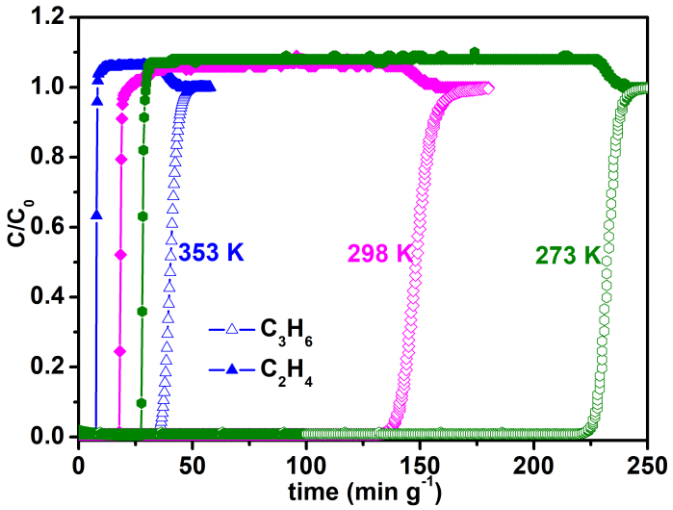

Figure S33. Breakthrough curves for C_3H_6/C_2H_4 (v/v, 4/36) mixtures at 353, 298 and 273 K.

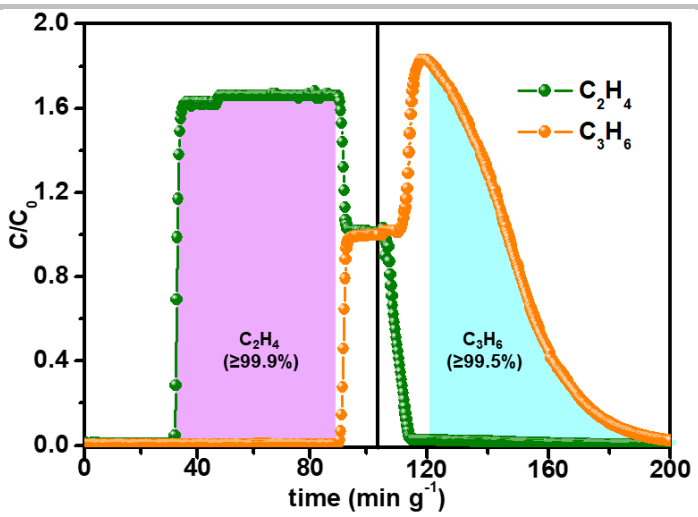

Figure S34. Breakthrough curves for C_3H_6/C_2H_4 (v/v, 20/20) mixtures at 273 K, followed by desorption curves under Ar (7 mL min^{-1}) sweeping at 323 K.

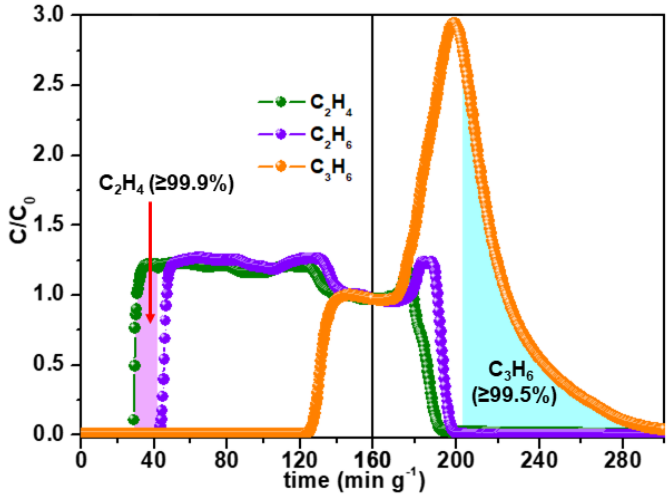

Figure S35. Breakthrough curves for $C_2H_6/C_3H_6/C_2H_4$ mixture (v/v/v,5/5/5) mixtures at 298 K, followed by desorption curves under Ar (7 mL min^{-1}) sweeping at 323 K.

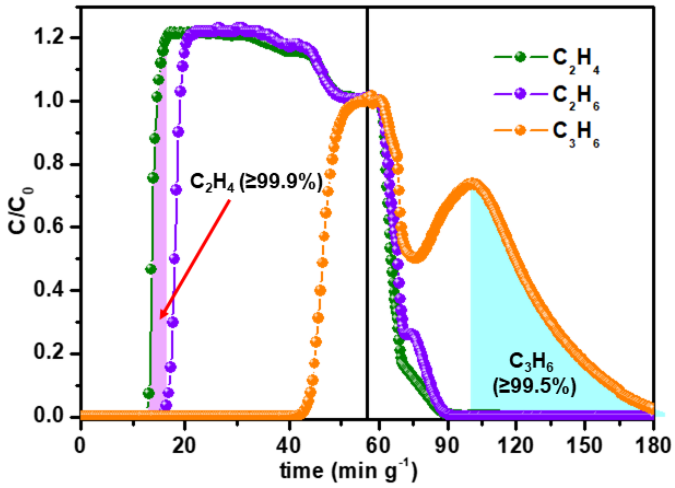

Figure S36. Breakthrough curves for $C_2H_6/C_3H_6/C_2H_4$ mixture (v/v/v,5/5/5) mixtures at 353 K, followed by desorption curves under Ar (7 mL min^{-1}) sweeping at 323 K.

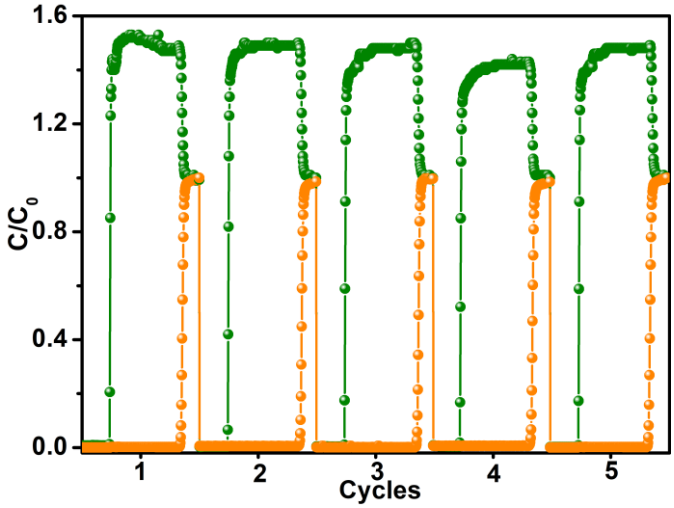

Figure S37. Breakthrough cycles of MAC-4 for C_3H_6/C_2H_4 mixtures at 298 K.

Transient breakthrough simulations vs experiments with inert gas

The transient breakthrough experiments were conducted with mass of MAC-4 m_{ads} = 0.88 g; length of packed bed, L = 80 mm; diameter of packed bed= 4.2 mm. The mixtures examined were:

C_3H_6/C_2H_4/Ar mixtures (20/20/60 v/v) with Ar as the carrier gas, and a total flow rate of 8.0 mL min^{-1} (353 K and 298 K, 100 kPa);

C_2H_6/C_2H_4/Ar mixtures (5/5/90, 1/9/90, and 1/15/84, v/v/v) with Ar as the carrier gas, and a total flow rate of 7 mL min^{-1} (353 K and 298 K, 100 kPa);

$C_3H_6/C_2H_6/C_2H_4$/Ar mixtures (5/5/5/85, 10/2/25/63, v/v/v/v,) with Ar as the carrier gas, and a total flow rate of 8 mL min^{-1} (353 K and 298 K, 100 kPa).

Transient breakthrough simulations were carried out for the exact same set of operating conditions as in the above mentioned experiments, using the methodology described in earlier publications.[2-7] In these simulations, intra-crystalline diffusion influences are ignored. There is good match between the experiments and simulations in every case.

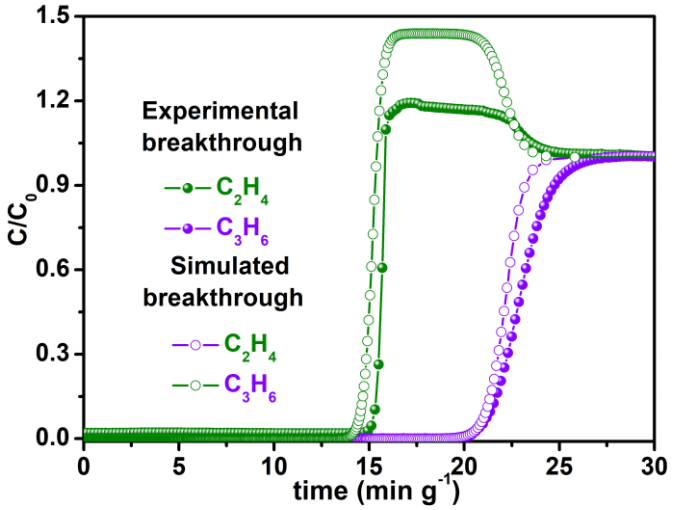

Figure S38. Comparison of the transient breakthrough curves and experimental breakthrough curves for C_2H_6/C_2H_4 (5/5) mixtures at 353 K.

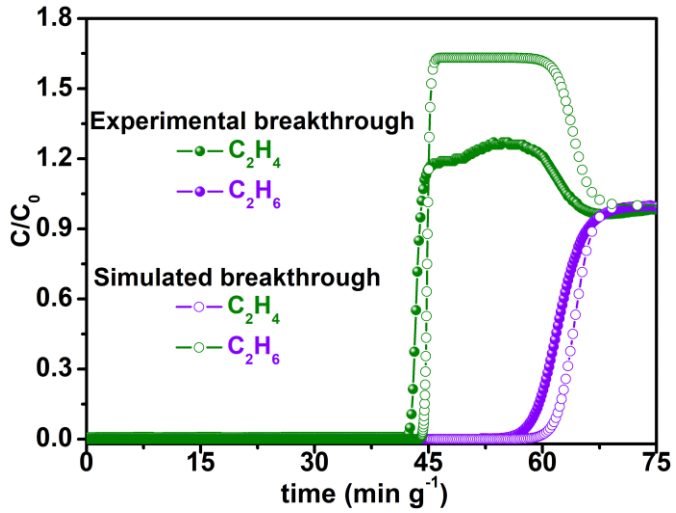

Figure S39. Comparison of the transient breakthrough curves and experimental breakthrough curves for C_2H_6/C_2H_4 (5/5) mixtures at 298 K.

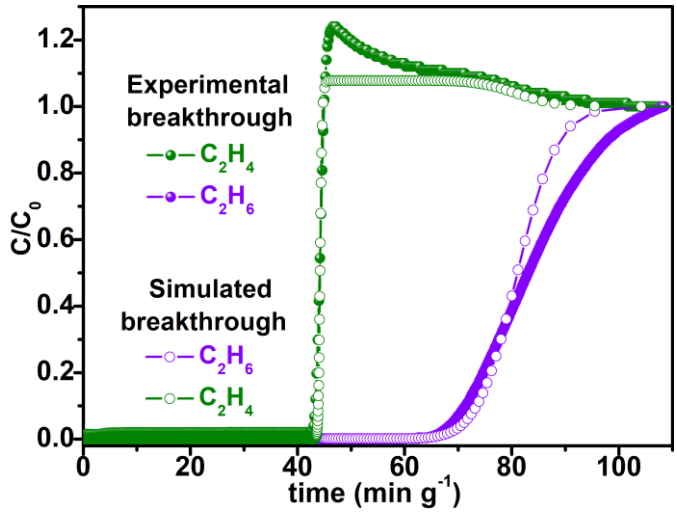

Figure S40. Comparison of the transient breakthrough curves and experimental breakthrough curves for C_2H_6/C_2H_4 (1/9) mixtures at 298 K.

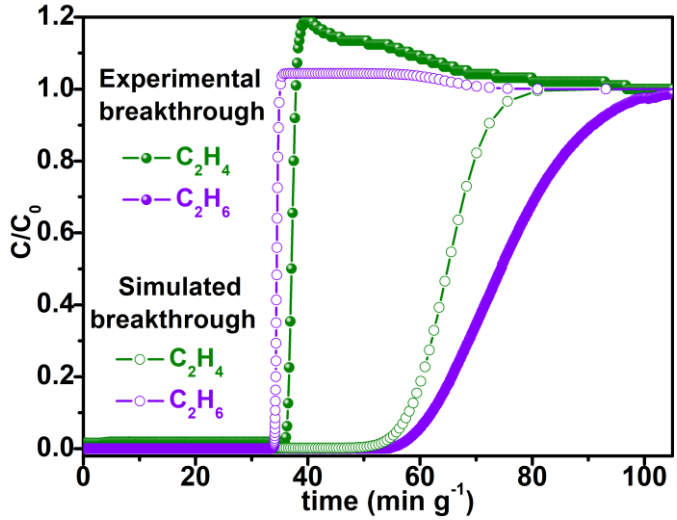

Figure S41. Comparison of the transient breakthrough curves and experimental breakthrough curves for C_2H_6/C_2H_4 (1/15) mixtures at 298 K.

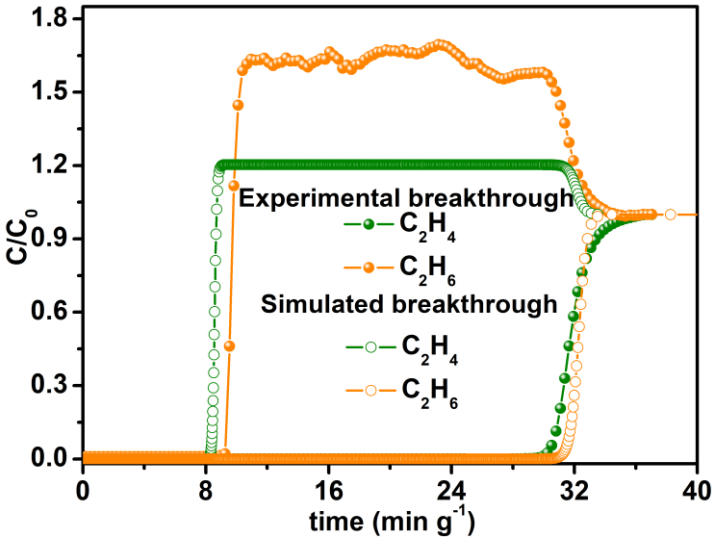

Figure S42. Comparison of the transient breakthrough curves and experimental breakthrough curves for C_3H_6/C_2H_4 (20/20) mixtures at 353 K.

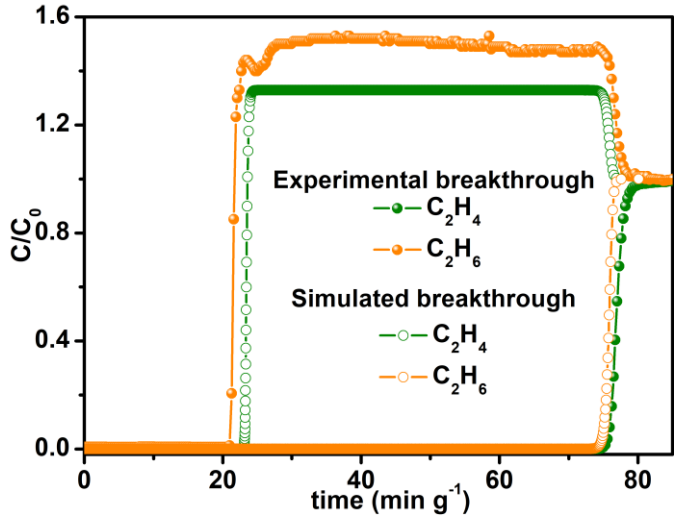

Figure S43. Comparison of the transient breakthrough curves and experimental breakthrough curves for C_3H_6/C_2H_4 (20/20) mixtures at 298 K.

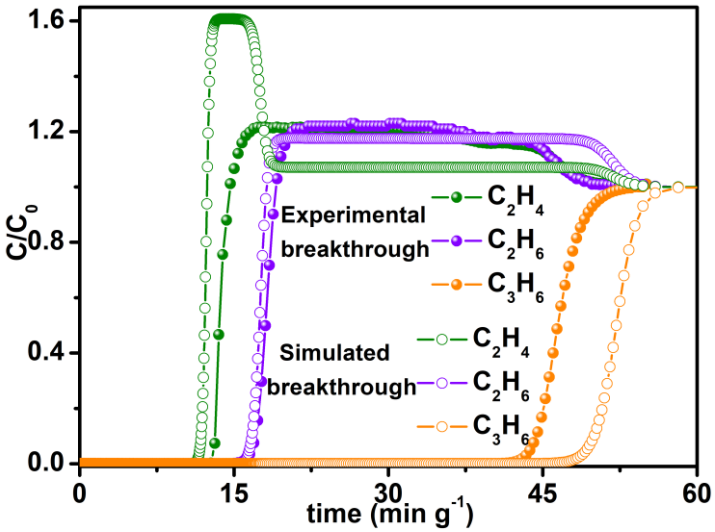

Figure S44. Comparison of the transient breakthrough curves and experimental breakthrough curves for $C_3H_6/C_2H_6/C_2H_4$ (5/5/5) mixtures at 353 K.

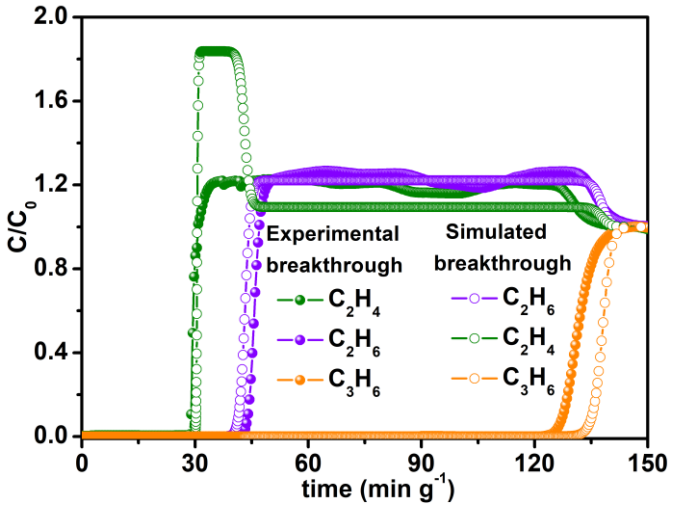

Figure S45. Comparison of the transient breakthrough curves and experimental breakthrough curves for $C_3H_6/C_2H_6/C_2H_4$ (5/5/5) mixtures at 298 K.

Transient breakthrough simulations without inert gas

Having established the accuracy of the transient breakthrough simulations, a set of simulations were carried out without inert gas in a fixed bed packed with MAC-4 m_{ads} = 0.88 g; length of packed bed, L = 80 mm; diameter of packed bed= 4.2 mm. The total pressure is 100 kPa, and two different temperatures were used: 298 K and 353 K. The following mixtures were simulated.

50/50 C_2H_6(1)/C_2H_4(2) mixtures

50/50 C_3H_6(1)/C_2H_4(2) mixtures

33.33/33.33/33.33 C_3H_6(1)/C_2H_6(2)/C_2H_4(3) mixtures

The breakthrough data are presented in terms of the dimensionless concentrations at the exit of the fixed bed, $\frac{c_A}{c_{A0}}$, as function of the modified time parameter $\frac{\left(Q_0 = \text{flow rate mL min}^{-1}\right) \times (\text{time in min})}{(\text{g MOF packed in tube})} = \frac{Q_0 t}{m_{ads}} = mL\ g^{-1}$.

From the transient breakthrough simulations, the productivity of 99.9% C_2H_4 was determined from a material balance.

Notation:

b	Langmuir constant, Pa^{-1}
E	energy parameter, J mol^{-1}
L	length of packed bed adsorber, m
m_{ads}	mass of adsorbent packed in fixed bed, g
p_i	partial pressure of species i in mixture, Pa
p_t	total system pressure, Pa
q_i	component molar loading of species i, mol kg^{-1}
q_t	total molar loading in mixture, mol kg^{-1}
q	component molar loading of species i, mol kg^{-1}
q_{sat}	saturation loading, mol kg^{-1}
Q_0	volumetric flow rate of gas mixture entering fixed bed, $m^3\ s^{-1}$
Q_{st}	isosteric heat of adsorption, kJ mol^{-1}
T	absolute temperature, K
u	superficial gas velocity in packed bed, m s^{-1}
ε	voidage of packed bed, dimensionless
ρ	framework density, kg m^{-3}

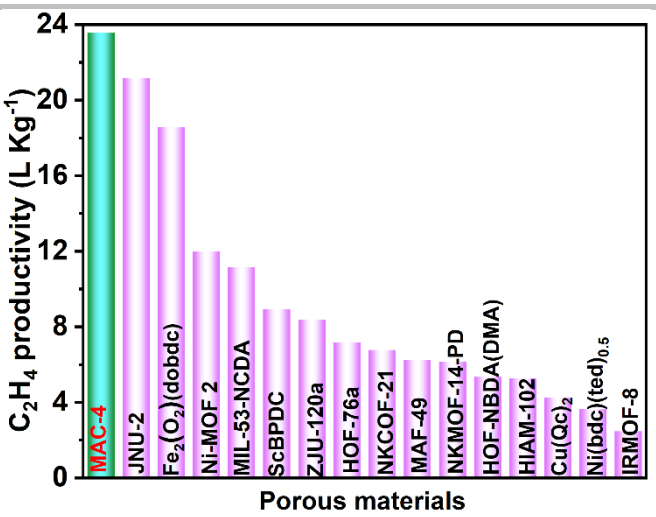

Figure S46. Comparison of C_2H_4 productivity form equimolar C_2H_6/C_2H_4 mixture in MAC-4 and reported porous adsorbents.

Infrared spectroscopy study

Infrared (IR) measurements were performed on a Bruker INVENIO S ATR-FTIR spectrometer. The samples of gas-loaded MAC-4 were prepared by the method described below: The sample of MAC-4 was filled into a glass tube and heated at 140 °C under vacuum for 4h. After the sample cooling down, C_2H_4, C_3H_6, and C_2H_6 was introduced into the sample respectively with Micrometrics TriStar II 3020 instrument until the pressure reach to 100 kPa at 298 K and the state is maintained for two hours. Then gas loading sample were picked out for infrared measurement immediately.

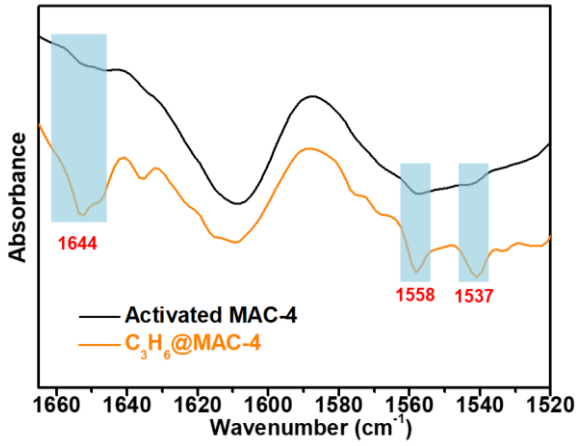

Figure S47. Comparison of IR spectra at 1660-1520 cm^{-1} of activated and C_3H_6-loaded MAC-4.

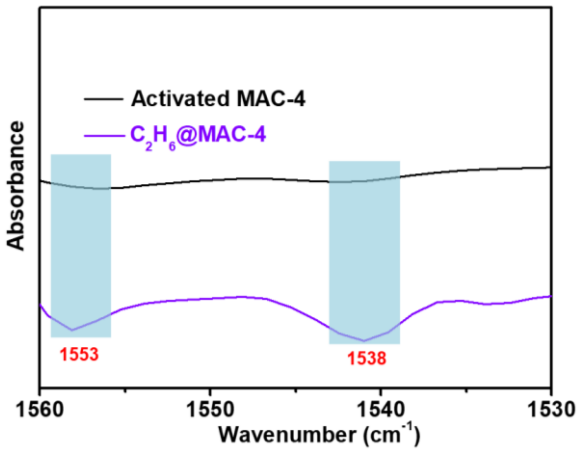

Figure S48. Comparison of IR spectra at 1560-1530 cm^{-1} of activated and C_2H_6-loaded MAC-4.

References

[1] Y. Ling, F. Yang, M. Deng, Z. Chen, X. Liu, L. Weng, Y. Zhou, *Dalton Trans*. **2012**, *41*, 4007-4011.

[2] *R. Krishna*, *RSC Adv.* **2017**, *7*, 35724-35737.

[3] R. Krishna, *ACS Omega* **2020**, 5, 16987−17004.

[4] R. Krishna, *Microporous Mesoporous Mater.* **2014**, *185*, 30-50.

[5] R. Krishna, *RSC Adv.* **2015**, *5*, 52269-52295.

[6] R. Krishna. *Sep. Purif. Technol.* **2018**, *194*, 281-300.

[7] R. Krishna. *Precision Chemistry* **2023**, *1*, 83-93.

Author contributions

Gang-Ding Wang: Synthesis, characterization, adsorption experiments, writing - original draft. **Yong-Zhi Li:** Breakthrough experiments, writing - review & editing. **Rajamani Krishna:** Breakthrough simulation**,** Q_{st} calculation. **Wen-Yan Zhang:** Formal analysis. **Lei Hou:** Formal analysis, writing - review & editing, supervision, methodology, funding acquisition. **Yao-Yu Wang:** Resources. **Zhonghua Zhu:** Formal analysis.